Thesis for the Degree of Master Engineering

Highly Stretchable and Water-Transience Cellulose/Conductive PEDOT:PSS Composite for Multifunctional Wearable Sensors

by

Anky Fitrian Wibowo

Department of Smart Green Technology Engineering

The Graduate School

Pukyong National University

February, 2022

Highly Stretchable and Water-Transience Cellulose/Conductive PEDOT:PSS Composite for Multifunctional Wearable Sensors

(다기능 웨어러블 센서를 위한 신축 및 수분 투과성 셀룰로오스/전도성 PEDOT:PSS복합 필름)

Advisor: Prof. Yong Hyun Kim

by

Anky Fitrian Wibowo

A thesis submitted in partial fulfillment of the requirements

for the degree of

Master of Engineering

in Department of Smart Green Technology Engineering,

The Graduate School

Pukyong National University

February, 2022

Highly Stretchable and Water-Transience Cellulose/Conductive PEDOT:PSS Composite for Multifunctional Wearable Sensors

A thesis
by
Anky Fitrian Wibowo

Approved by:

Kwon Taek Lim, Ph.D. (Chairman)

Kang-Jun Baeg, Ph.D. (Member)

Yong Hyun Kim, Ph.D. (Member)

February, 25th 2022

Table of Contents

List of Tables

List of Figures

다기능 웨어러블 센서를 위한 신축 및 수분 투과성 셀룰로오스/전도성 PEDOT:PSS 복합 필름

Anky Fitrian Wibowo

부경대학교 대학원 스마트그린기술공학과

요약

피부에 부착할 수 있는 전도성 전극 재료는 웨어러블 소자 및 생체 신호 모니터링 등의 응용 분야에서 주목받으며 연구되고 있다. 피부와 유사한 유기 전도성 필름을 제작하기 위해서는 피부 순응성, 신축성, 움직임과 생물학적인 신호에 대한 민감성 및 기계적/전기적으로 견고한 특성이 요구된다. 본 연구에서는 Poly(3,4-ethylene dioxythiophene): poly(styrene sulfonate) (PEDOT: PSS)을 전도층으로 사용하여 전도성, 신축성, 수분해성 및 민감도가 높은 셀룰로오스 필름을 제작하였다. PEDOT:PSS는 에틸렌 글리콜과 계면활성제 FS-31을 사용하여 습윤성과 전도성을 향상시켰다. 또한, 신축성 기판의 표면 개질제로 11-aminoundecanoic acid (11-AA)를 셀룰로오스 기판과 PEDOT:PSS 사이에 도입하여 화학적 결합을 강화함으로써 기계적/전기적 특성을 개선하였다. 신축성 셀룰로오스/PEDOT:PSS 복합체는 높은 피부 친화성과 감도 특성으로 체온과 호흡 등과 같은 생리학적인 변화를 인지 할 수 있다. 본 연구의 신축성, 생분해성, 피부 부착성의 셀룰로오스/PEDOT:PSS 복합 필름은 헬스케어 모니터링을 위한 차세대 웨어러블 센서의 핵심적인 소재 기술이라고 판단된다.

키워드: 생분해성, 셀룰로오스, PEDOT: PSS, 센서, 웨어러블 소자

Highly Stretchable and Water-Transience Cellulose/Conductive PEDOT:PSS Composite for Multifunctional Wearable Sensors

Anky Fitrian Wibowo

Department of Smart Green Technology Engineering
Graduate School of Engineering
Pukyong National University

Abstract

Skin-attachable conductive electrodes are an attractive research area for wearable devices and physiological monitoring applications. Organic skin-like conductive films must have perfect on-skin conformability, stretchability, outstanding sensitivity to motion and biological signals, and also highly robust mechanical/electrical characteristics. This study designed a conductive, stretchable, hydro-biodegradable, and highly sensitive cellulose film integrated with poly(3,4-ethylene dioxythiophene): poly (styrene sulfonate) (PEDOT: PSS) as the conductive layer. PEDOT: PSS optimized by ethylene glycol (EG) and non-ionic fluorosurfactant FS-31 to improve wettability and conductivity. Surface modifier 11-aminoundecanoic acids (11-AA) strengthen the chemical interaction between cellulose and PEDOT: PSS, resulting in reliable mechanical/electrical properties. Stretchable cellulose/PEDOT: PSS with its compatibility and sensitivity properties integrated with human skin to record physiological activities as well as temperature and breath humidity intensity. We believe that stretchable, biodegradable, skin-attachable cellulose / PEDOT:PSS film can be a trustworthy candidate as wearable sensor applications.

Keywords: Biodegradable, Cellulose, PEDOT: PSS, Sensors, Wearable Devices

I. Introduction

Biodegradable and skin-attachable materials are convincing research in the advanced era of wearable technologies such as healthcare monitoring and e-skins sensors that are eco-friendly, high skin-conformability, non-toxicity and lightweight. PEDOT: PSS looks attentively as a conductive layer with high electrical conductivity, good durability, excellent chemical stability and outstanding geometrical responsiveness[1–3] that developed as a strain-responsive[4,5], human skin[6], sweat[7], temperature[8–10], and humidity sensors[10,11]. PEDOT: PSS has been integrated with a variety of stretchable biopolymers, including chitosan[6] , polydimethylsiloxane (PDMS)[12,13], and polyurethane (PU) [4,14] with limited biodegradability. Biodegradation and sustainability must be thoroughly considered to counteract adverse effects on the biophysical system by exploring green electronics potential[15]. The researcher created green electronics by combining stretchable cellulose with the conductive polymer PEDOT: PSS. Cellulose is an organic polysaccharide molecule derived from green plant cell walls. The hydroxyethyl cellulose (CH_2CH_2OH) derivative of cellulose is widely used as a gelling agent. Cellulose tends to be non-stretchable, brittle, and low-strain performance[16] which is unable to realize strains up to above 20%[17] so it requires plasticizers such as urea[17], glycerol[18], polyvinyl alcohol[19] to offer additional bonding and boost stretchability.

Here, we reveal a stretchable cellulose/PEDOT: PSS composite film as being hydro-biodegradable, on-skin conformable, and has a high electrical sensitivity for multifunctional wearable sensors such as monitoring physical activity in the human body, temperature, and humidity levels emerging from the respiratory system. The addition of reducing agent ethylene glycol (EG) is necessary because PSS counterions will inhibit the conductivity pathway. EG alters the structure of the PEDOT: PSS chains as a secondary dopant and enhances electrical conductivity up to three times.[20,21]No less important, the use of the right surfactant greatly lowers the contact angle and surface tension between PEDOT: PSS/organic substrates and increases wettability, allowing PEDOT: PSS to be distributed uniformly[22,23]. The functionalization of 11-aminoundecanoic acid (11-AA) on the cellulose surface is expected to improve the interfacial adhesion, optical and electrical properties between PEDOT: PSS and cellulose substrate[6,24]. This study has successfully designed a high sensitivity multifunctional wearable sensor for physiological activities, temperature, and humidity, which can be actualized as a candidate for green wearable electronics.

II. Theoretical Basis

1. Wearable Devices

As the beginning of next-generation technology, flexible and stretchable electronics are garnering a great deal of attention in entire electronic systems because of their resistance to stress-strain forces and conformability to various surfaces. Then, stretchable electronics subjected as skins sensors, artificial skins, stretchable energy conversion, and numerous new functionalities[25,26].

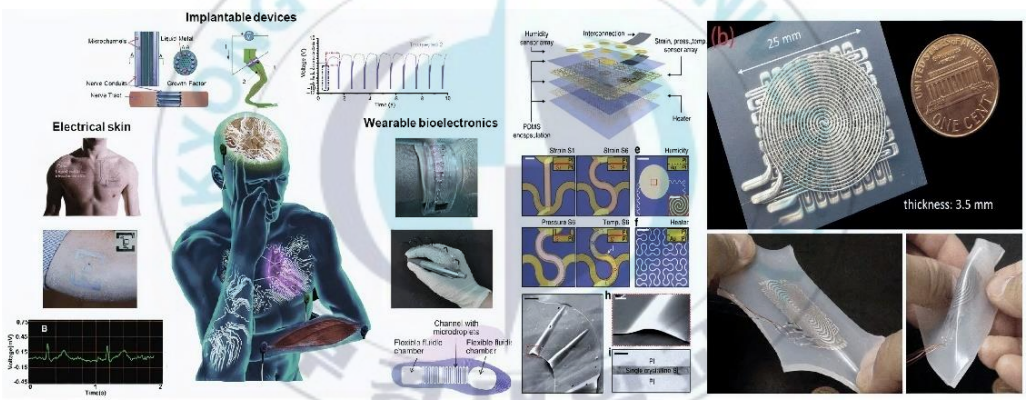

Figure 1. The potential of flexible and stretchable electronics for wearable devices and artificial skin[27–29].

Stretchable, soft, and skin-integrated electronics open up new opportunities to be implemented with soft tissues for future research direction on robotic controlling and health monitoring for clinical evaluation of specific diseases[30]. Polyurethane (PU), polydimethyl-siloxane (PDMS), and styrene-butadiene rubber (SBR) are renowned

elastomeric substrates used in electronic systems and are possible to maintain up to 200% of stretching[25].

Several tactics are used to improve the performance of stretchable devices such as wavy structural configuration[31], island interconnects and mesh structure[32], origami and kirigami configuration[33,34]. Furthermore, conductivity and uniform ability enhanced by utilizing metal nanoparticles, metal nanowires, carbon nanotubes, conductive polymer, and others with diverse strategies such as spin-coating, blending, printing, and others methods. These strategies are constantly optimized in order for flexible and stretchable electronics to maintain performance when subjected to continuous 2D/3D mechanical stress deformation[33].

2. Green Electronics

Figure 2. Green electronics illustration[34].

The electronic revolution in this century impacts how we live harmoniously with various technologies such as smartphones, laptops, solar cells, LEDs, sensors, and others. As electronic functionalities broaden, there is a growth in high market demand and high energy consumption in the manufacturing process, resulting in an energy imbalance. Various consequences occurred, such as waste of electrical and electronic equipment (WEEE), natural material crises of gallium and indium, which expected to run out in the next 20 years. This WEEE problem seems to be quite concerned, for example, China, Japan, the United States, and the European Union are the primary contributors up to 50 million tons per year, so the United Nations has drawn attention to publicize SDG No. 12 on responsible production and consumption to strengthen sustainable development. The ever-increasing volume of electronic waste contaminates water, soil, and air in several countries, causing negative effects on biosystem and environmental issues. Popular semiconductor materials used such as chromium (Cr), lead (Pb), and Arsenic (As) contain toxic elements that harm the environmental balance[35–37].

Green electronics openly supports the potential of organic materials, which provide energy-efficient materials, low costs, and future electronic function opportunities. Organic materials offer great benefits over inorganic materials, such as flexibility, high conformability, non-toxicity, and excellent biodegradability, making them suitable for integration with human body systems for healthcare applications and

biomedical monitoring[36,37]. Eco-friendly and renewable bioplastics such as cellulose, thermoplastic starch, chitosan, and polylactic acid are expected to be reliable candidates for green electronics because of their biodegradability either through hydrolysis or enzymatic reactions that break up the main structure[38,39]. One of the concepts is to create sustainable and eco-friendly electronics by assembling electronic components from cellulose, a polysaccharide derivative found in plant cell walls. Hydrolysis reactions and fungal biodegradation can completely degrade cellulose. Furthermore, it has the potential to improve its flexibility, transparency, mechanical, and electrical properties. As previously reported, cellulose attracts the research interest as an electronic device, such as the green chip of microwave and digital electronics[39], supercapacitor[40], transistor[41], flexible memory[42], and others. Green electronics that are low-cost and low-energy must be manufactured on an industrial scale to advance optoelectronic and wearable devices as well as reduce waste generation for biosystem stability.

3. Conductive Polymer

Conductive polymers have a long conjugate chain structure that is constituted of double bonds and heteroatoms. Because of the л to л-electron transformation of double bonds and their heteroatoms, polymers have a conductive characteristic. The intramolecular bonds in polymers are strong, but the intermolecular bonds are weak.

Electrons and holes are charge carriers that determine polymer conductivity and can be controlled by doping agents that provide electron donors/acceptors so that the excessive electrons or electron holes allow the electric current to travel. Conductive polymers are frequently referred to as semiconductor materials, and some examples include polyacetylene (PAC), polyanilines (PANi), polypyrrole (PPy), and poly(3,4-ethylenedioxythiophene) (PEDOT), which are influential in the growth of semiconductor devices[42].

3.1 Polyacetylene

Organic polymer polyacetylene (PA) is the first potential as a representative organic semiconductor developed by Hideki Shirakawa, Alan Heeger, and Alan MacDiarmid, who won the Nobel Prize in 2000. PA is an organic polymer with a relatively simple conjugation system that has been widely used in various applications of semiconductor devices[43].

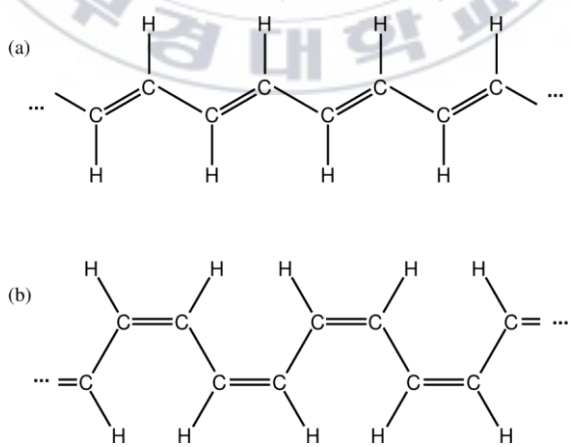

Figure 3. Polyacetylene structures conformations **a)** *trans*-PA and **b)** *cis*-PA[44].

Polyacetylene is a one-dimensional periodic system consisting of repeated C_2H_2 units with alternating short and long C-C bonds. PA exists in two forms: *cis* and *trans*, with trans-PA being more thermodynamically stable at room temperature[44]. Electrical stability has been achieved through argon (Ar) plasma treatment, which lessens the *cis* configuration while enhancing the *trans* configuration as Ar plasma power is increased[45]. Different models describe the electrical properties of polymers by the presence of delocalized charge carriers that propagate along the polymer backbone, namely pairs of solitons, polarons, and bipolarons[46]. Because of its good thermal decomposition resistance and efficient blue light emission, disubstituted polyacetylene is suitable for chemo sensor applications such as detecting copper (Cu) ions and α-amino acids to emerge as a viable candidate for optoelectronic applications[45].

3.2 Polyanilines

Polyaniline (PANI) is a promising conducting polymer candidate due to its simple electrochemical polymerization process, redox properties, environmental stability, tunable properties, low cost, and ease of electrode deposition[47,48].

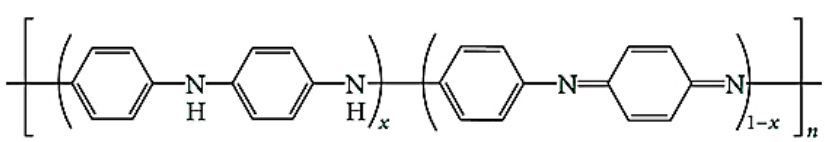

Figure 4. General structure of polyaniline base (PANI) [48].

PANI is a para-linked phenylene amine imine structure. In the general structure, there is $(1-x)$, and if $(1-x)$ is 0, the polymer has no such oxidized groups (is fully reduced) and is known as leucoemeraldine base (LE). If $(1-x)=1$, the polymer is fully oxidized with imine links instead of amine links and is known as pernigraniline base (PG). Specifically, when $(1-x)=0.5$, the emeraldine oxidation state (PANI base) is generated in which the number of reduced and oxidized units is the same[47,48]. Emeraldine base is the most functional type due to its high room temperature stability and doping to form emerald salt, which is more electrically conducting than LE and PG[47].

PANI is a p-type semiconductor with the majority of charge carriers being holes. The semi-conducting properties are influenced by the delocalization of the л bonds. When PANI is doped with acid, polaron is formed by the formation of successive bipositive species, bipolaron structure, and more stable polaron. This polaron structure facilitates electrical conduction through a hopping mechanism[49]. When emeraldine base is doped with aqueous protonic acid, the conductivity increases up to 10-fold and the color changes from blue to green. Polyaniline conductivity increases exponentially with temperature, and at temperatures above 300 K, PANI will obey Ohm's law. Temperature dependence occurs as a result of a combination of metallic islands and microscopic disorders[50].

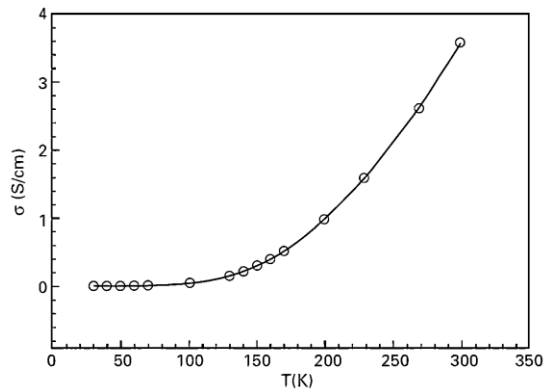

Figure 5. Conductivity-temperature function of PANI[50].

3.3 Polypyrrole

Polypyrrole (Ppy) has been widely reported as a conducting polymer in the presence of pi-electron conjugation for the detection of target analytes such as enzymes, nucleic acids, or antibodies[51]. Lan Qu et al reported electrochemically synthesized Ppy-Au nanoparticle composites for micro potentiometric hemoglobin immunosensors. Because of its high chemical stability, compatibility with immunoactivity entities, and support for nanoparticle doping, Ppy is a reliable candidate for immunosensor[52].

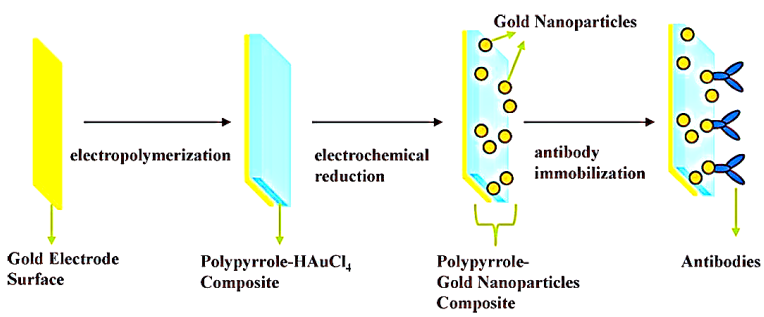

Figure 6. Scheme of antibody immobilization based on Ppy-Au nanoparticles[52].

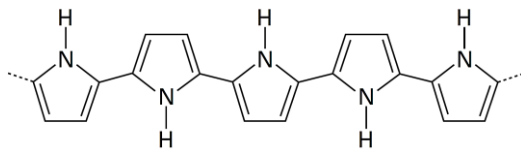

Figure 7. Molecular structure of polypyrrole (Ppy) [46].

Ppy has a chemical structure that is composed of repeating units of the py monomer and a nitrogen-containing aromatic ring. Because of its p-type conduction, Ppy has good electrical conductivity and can be chemically modified to be better conjugated with biomolecules[53]. Ppy is complicated due to several limitations such as non-thermoplasticity, brittleness, rigidity, and non-biodegradability, and insoluble in common solvents[54]. Mechanical and processability properties have been developed to overcome brittleness issues in Ppy, such as blending Ppy with numerous polymers or forming Ppy copolymers. Some doping, such as anion surfactants, can boost Ppy conductivity and can be deposited on various metal and nonmetal substrates[46].

Table 1. Polypyrrole conductivity based on different oxidizer/dopants[46].

Oxidiser/dopant	Conductivity, [Ω m] $^{-1}$
$FeCl_3$	0.02 [21]
$CuCl_2$	$6 \cdot 10^{-7}$ [21]
DBSA (dodecylbenzenesulfonic acid)	0.01 [24]
$Fe_2(SO_4)_3$	$3.9 \cdot 10^{-4}$ [23]
$Fe_2(SO_4)_3$: AOT (20:1)	0.045 [23]

3.4 Poly(3,4-ethylenedioxythiophene)

Poly-3,4-ethylenedioxythiophene (PEDOT) is a conductive polymer with a heterocyclic thiophene ring structure linked by a diether. One of the advantages is the ease of processability and can be deposited on various conductive and non-conductive substrates[46]. The PEDOT layer especially exhibits a highly ordered crystal microstructure with high anisotropy and parallel to the substrate.

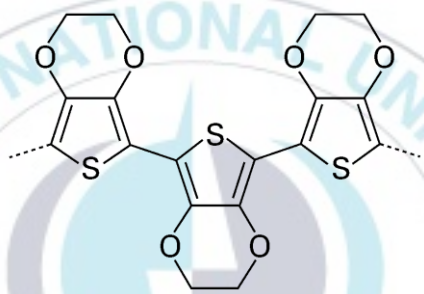

Figure 8. Chemical structure of poly-3,4-ethylenedioxythiophene (PEDOT) [46].

PEDOT has a narrow bandgap by the presence of two electron-donating oxygen atoms adjacent to the thiophene unit. Commercially, PEDOT is combined with poly(styrene sulfonate) (PSS) in water and is appropriate to film deposition. The delocalization of л-electrons in the chemical structure and the presence of sulfonated polystyrene (PSS) are responsible for electrical conductivity. PEDOT:PSS able to support electronic and ionic conduction, outstanding electrochemical stability, high biocompatibility, and transparency performance of up to >90% in optoelectronic and wearable device applications[55,56]. The conductivity of PEDOT:PSS is significantly

impacted by phase-separated morphology, PEDOT crystallization, removal of insulating PSS, and PEDOT oxidation, and others. Organic solvents such as ethylene glycol (EG), dimethylsulfoxide (DMSO), sulfuric acid (H_2SO_4), and ionic liquids are used in doping treatments. According to Xi Fan *et al*, EG doping and additional plasma O_2 treatment is the best treatment for optimizing PEDOT:PSS (PH1000) conductivity to 5012 S/cm[57]. Furthermore, the shearing method with EG yields a conductivity of up to 4600 S/cm with a transmittance of 97%[58].

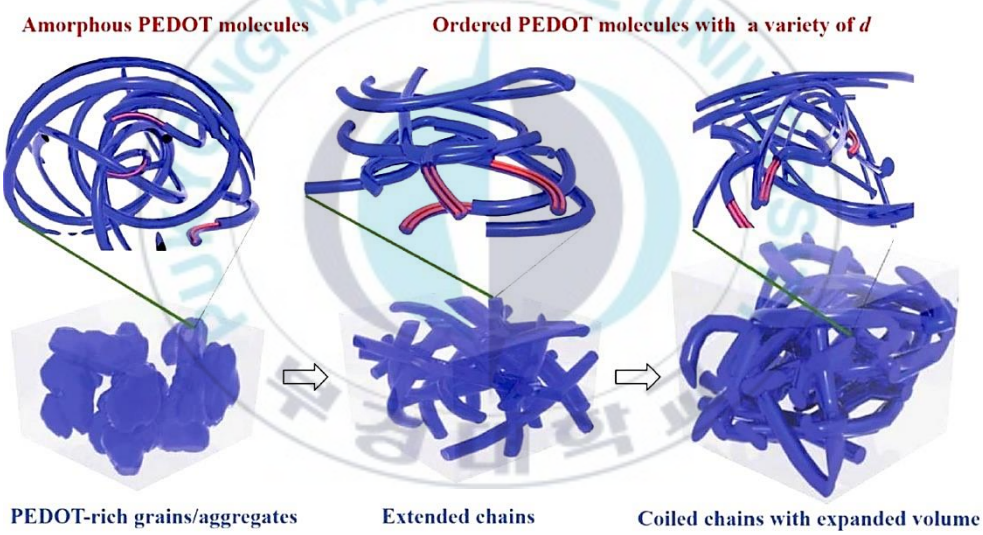

Figure 9. Schematic of structural rearrangement of highly conductive PEDOT:PSS[59].

The attraction between positively charged PEDOT and counterions PSS in the pristine films led to coiled PEDOT and PSS chains encircled by PSS shells. PSS acts as a barrier, restricting charge transfer within the PEDOT network. The static charge interaction between PEDOT and PSS was disrupted by EG, causing a realignment to

become more ordered. Because of the continuous pathways and smaller PSS barriers, current flow becomes more efficient[57]. In addition to doping with organic solvents, there are various techniques for increasing the conductivity of PEDOT: PSS include post-treatments with polar solvent doping, ionic liquid treatments such as 1-butyl-3-methylimidazolium tetrafluoroborate ((BMIm)BF4) / 1-ethyl -3-methylimidazolium tetracyanoborate (EMIM:TCB) and strong acid soaking treatments such as H_2SO_4[60] and HNO_3[61] so that H^+ ionizes from acid and combines with PSS^- to form neutral PSSH[59].

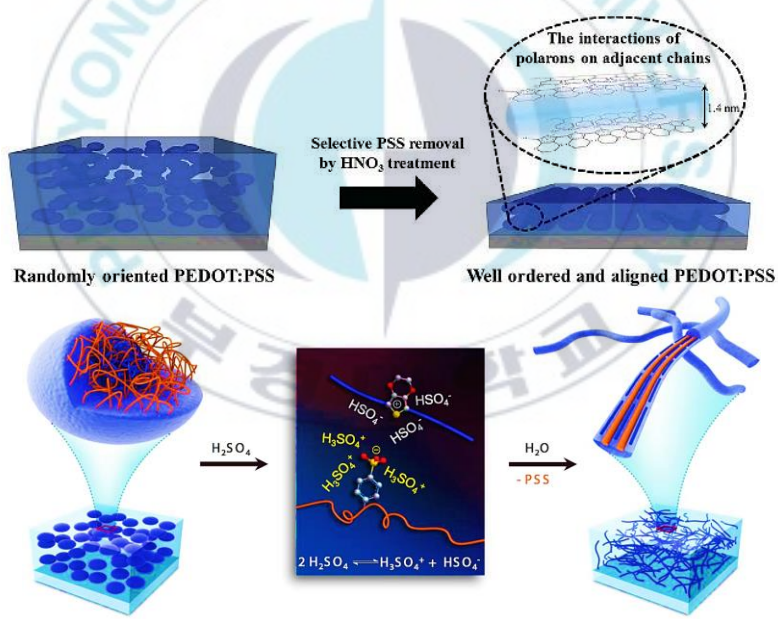

Figure 10. Mechanism of strong acid soaking treatments by HNO_3[61] and H_2SO_4[60]

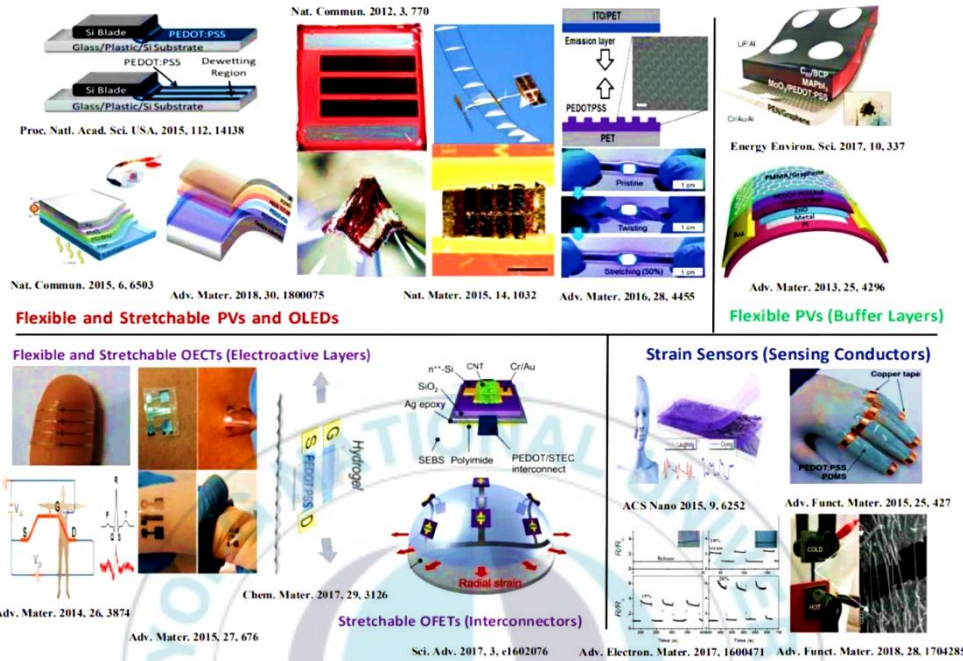

Figure 11. The milestone of flexible and stretchable device based on PEDOT:PSS[59].

PEDOT:PSS has been integrated with various flexible substrates in recent years for strain sensors, organic light-emitting devices, stretchable organic field-effect transistors, and other devices. PEDOT:PSS offers countless challenge prospects to further develop its properties, indicating that it has a positive vision in the innovation of wearable and optoelectronic devices.

Table 2. Summary of Conductive Polymer[51].

Conductive Polymer		Application	Mechanism	Performance
Polyacetylene **PAC**	Disubstituted polyacetylene	α-amino acids detection	α-amino acids interrupt the connection of Cu ions-imidazole moieties and the quenched fluorescence could recover	Detection limit: 6×10^{-5} mol/L
Polyaniline **PANi**	PAn-Cl PAn-Br PAn-ClO_4	Detection of organic and inorganic solvents such as EtOH, C_6H_6, HCl, NH_3 and $CHCl_3$	Protonation-deprotonation with the advent of -NH group in the polymer backbone resulted in a change in the electrical conductivity as well as in the color of the polymer	Conductivity: 1. 0.35 S/cm 2. 0.69 S/cm 3. 1.10 S/cm
Polypyrrole **PPy**	Electro polymerized PPy	Hydrogen gas sensing	The interaction between Ppy sensitive films and the adsorbed gas molecules can lead to a homogeneous charge transfer	Response time 50-90s
	Overoxidized PPy	Dopamine determination	Oxidation of dopamine at the OPPy-modified sol-gel derived bioelectrode	Response range 9.99×10^{-6} – 1.1×10^{-3} M
	PANi-Ppy zirconium titanium phosphate	Chemical sensor	The dopant that stabilizes the polaron and bipolaron states as counter anions resulted in high electrical conductivity	Conductivity: 10^{-5} – 10^{-3} S/cm
	Ppy nanotubes	Glucose detection	Liquid-ion gated field-effect transistor configuration	Response range: $0.5 - 20 \times 10^{-3}$ M
Poly-3,4-ethylenedioxy thiophene (PEDOT)	Poly-3,4-ethylenedioxy thiophene	1. Glucose Detection 2. Determination of ascorbic acid and dopamine	PEDOT was used as a matrix for entrapping glucose oxidase Electrostatic reaction between positively charged of polymer film and negatively charged of ascorbate anions shifted their oxidation potential to a less positive potential whereas as the dopamine oxidation potential was not shifted due to hydrophobic interaction	Sensitivity: 12.42 mA/M/cm^2 Response time: 4-10s Sensitivity: 0.012 uA/uM and 0.022 uA/uM for ascorbic acid and dopamine, respectively
	Poly-3,4-ethylenedioxy thiophene/ poly(styrene sulfonic acid)	Determination of dopamine	Organic electrochemical reaction	Detection limit: <5 nM
	Polytyramine	Simultaneous and selective determination of dopamine and ascorbic acid	The modified electrode had a reactivity and sensitivity in the oxidation of dopamine and ascorbic acid	Detection limit: 142 nM and 331 nM for dopamine and ascorbic acid

4. PEDOT:PSS-Based Sensor

4.1 Strain-Responsive Sensor

Sensors are fascinating semiconductor applications because they respond to biological, chemical, and physical phenomena, which are then transformed into electrical variables that can be measured. PEDOT: PSS has attracted attention due to its excellent electrical and structural properties. Piezoresistive property of PEDOT:PSS can affect its resistance when there is geometric deformation and reduce the cross-section of the active material, causing an increase in resistance in the PEDOT:PSS layer. The sensitivity between resistance and strain is evaluated by the gauge factor (GF). The gauge factor has the following equation,

$$\varepsilon_r = \frac{(L - L_0)}{L_0} \quad (1)$$

$$R_n = \frac{(R - R_0)}{R_0} \quad (2)$$

$$GF = \frac{R_n}{\varepsilon_r} \quad (3)$$

Strain (ε_r) is the ratio of the difference in length increase with the initial length, then electrical resistance (R_n) is the ratio of the difference in resistance during extension (R) and without extension (R_0) [62]. Adhesion properties are crucial to maintaining stability between the PEDOT: PSS layer and the stretchable substrate, allowing it to function as a strain responsive sensor for a long time. To boost GF in piezoresistive

sensors, the high resistive path caused by the current-induced PEDOT:PSS phase segregation can be designed perpendicular to the strain sensing direction[63]. Electrical conductivity depends on the volumetric fraction of the defects and the percolation threshold. The deformation reduces the effective volume fraction of the PEDOT:PSS due to the formation of discontinuities and defects which can diminish the conductive channel. During releasing, the cracks can be reconnected thus causing the drop of resistance. Reversible disconnection-reconnection of cracks endows the strain sensor with high sensitivity and repeatability.

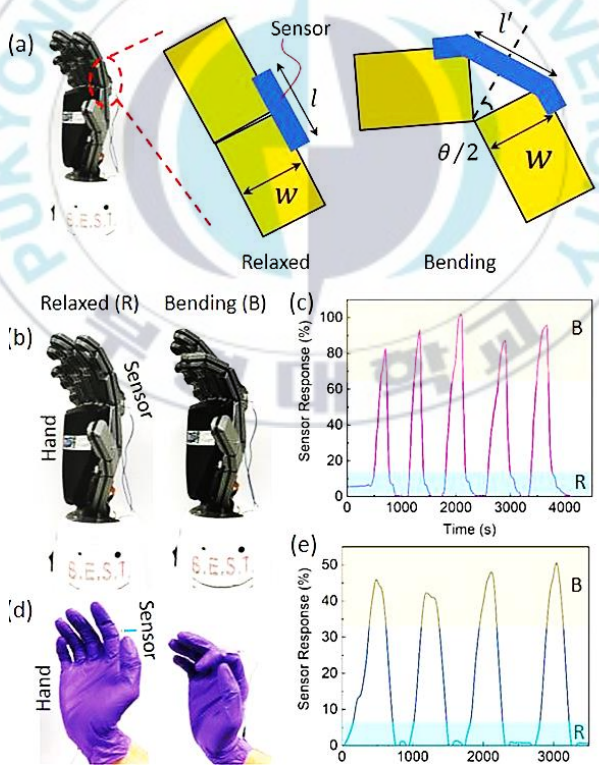

Figure 12. Sensor performance due to finger bending of the robotic and human hand[2].

The gauge factor can be calculated using the relationship between bending angle and stretching, and it can be used as a standard for sensing performance[2]. Human-skin sensors, health monitoring, and human-machine interactions could all benefit from flexible and elastic strain sensors.

4.2 Temperature-Resistance Function

PEDOT:PSS is shown to be a promising candidate for wearable temperature sensors due to its superior mechanical properties and tunable electrical characteristics, as well as its ease of manufacture and great reproducibility. In, semiconductor, there insufficient mobile carriers at low temperature and low resistance. When heated, more of the lightly bond carriers escape and become free to conduct or mobile carriers are fully activated.

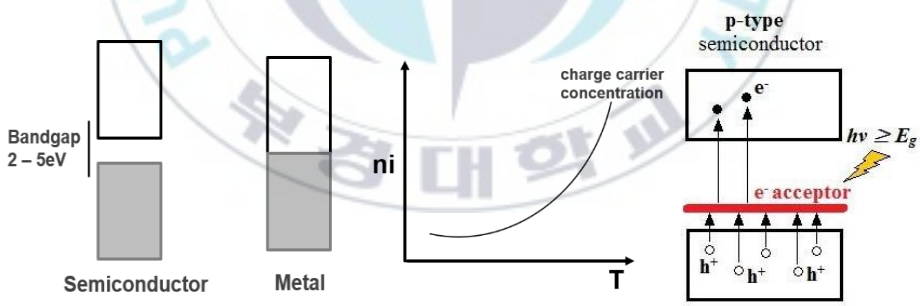

Figure 13. Bandgap and charge carriers as a function of temperature.

At high temperatures, the fermi level rises slightly upwards since $m_h > m_e$ then the electron from the valence band shifted to the conduction band across the bandgap and the carrier concentration increased. At low temperatures, the donor ionization

dominates the carrier density and the fermi level lies exactly in the middle. Temperature dependence is related to activation energy by fitting the carrier density vs 1/T with this formula[64,65],

$$n_0(T) = C \exp\left(-\frac{E_g/2}{kT}\right) \tag{4}$$

$$f(E) = \frac{1}{1+e^{\frac{-(E_f-E)}{kT}}} \tag{5}$$

As the temperature rises, thermal energy is released, allowing for more limited carrier hopping and tunneling both inside the grain and between neighboring nanosheets. The temperature sensor's sensitivity is defined by its temperature coefficient of resistance (TCR), which may be estimated [9].

$$TCR = \frac{R-R_0}{R_0} \times \frac{1}{\Delta T} \times 100\% \tag{6}$$

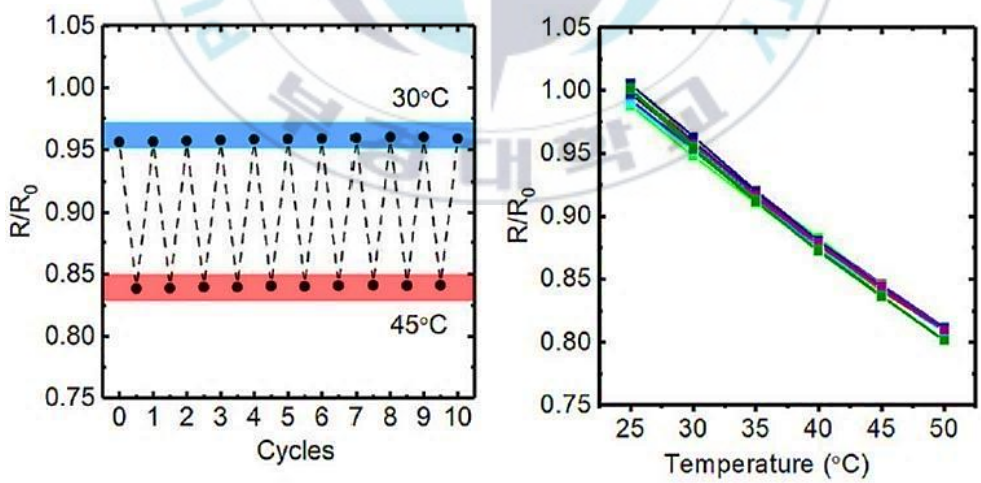

Figure 14. Relative resistance changes of printed temperature sensor under cyclic heating and cooling run [9].

Temperature dependent relative resistance changes of 10 cycles printed

temperature sensors. PEDOT:PSS showed relatively small response fluctuations, indicating that the sensor functioned well in a variety of temperature cycles and has good reproducibility [9]. The PEDOT:PSS-based temperature sensor comes from a microstructure known as core-shell structured grains, in which the grain's center is a PEDOT nanocrystal and a PSS-rich shell surrounds it. At high temperatures, the total number of particle boundaries is smaller and the effective size of the bonds is reduced which will decrease the resistance. When the temperature drops, the electron may not have enough thermal energy to overcome these barriers, causing the resistance to rise[65,66]. Wearable temperature sensors that can be integrated with the human body have attracted intense attention for continuous monitoring of temperature changes due to the onset of infections and diseases.

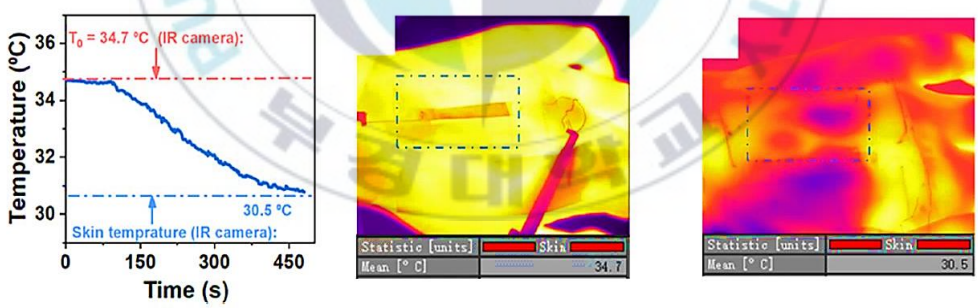

Figure 15. Monitoring skin temperature of palm with IR thermograms [66].

4.3 Humidity Sensor

The innovative humidity sensing configuration can control and detect ambient humidity, which is beneficial for environmental, health, and medical monitoring, as well as industrial processes [67]. PEDOT:PSS is a naturally water-absorbing polymer that responds linearly to changes in relative humidity from 20% to 80% and loses its sensing function when relative humidity surpasses 80% [68]. The sensor's working mechanism is based on physical adsorption-desorption. In particular, the PEDOT:PSS layer adsorbs water molecules as the ambient humidity rises, causing the sensor's resistance to change. Diffusion of H_2O into PEDOT:PSS drives swelling and dissociation of PEDOT and PSS bonds, leading to higher bond energy between PEDOT chains, which subsequently induces the protonation of SO_3H^+ groups at the PEDOT-PSS interface terminating in the creation of $H_3O^+ + PSS(SO_3)^-$ [69].

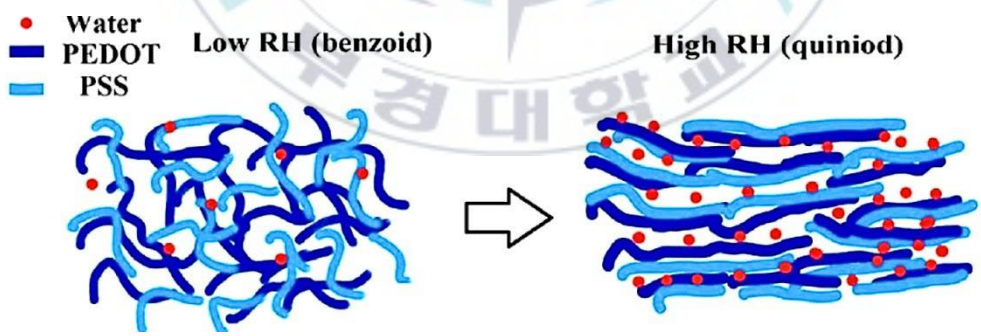

Figure 16. Schematics of the PEDOT:PSS sensing mechanism [11].

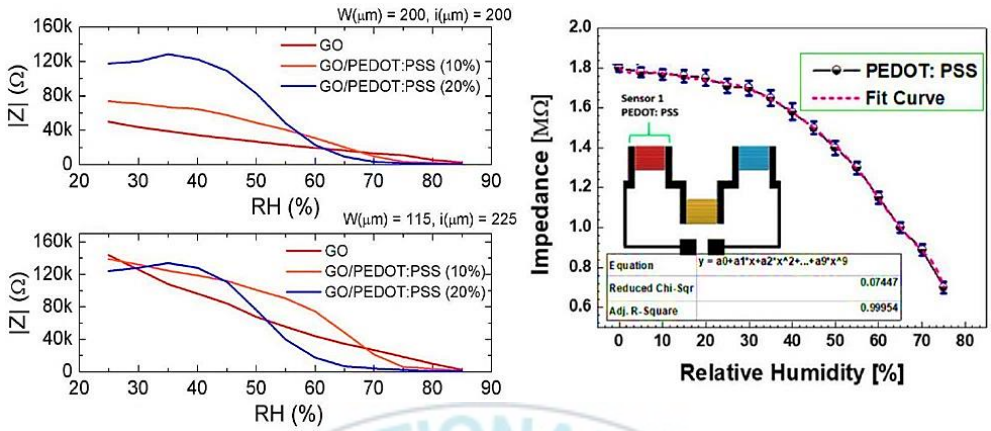

Figure 17. Impedance value as a function of the relative humidity [11,70].

Water molecules were ionized due to electrostatic field on the PEDOT:PSS surface forming hydronium ions (H_3O^+), thereby promoting the ionic conductions. At higher humidity levels, the hydroxyl groups in H_2O can create coulomb interaction with PEDOT. Boosting its positive charge carrier density and transforming the PEDOT structure from benzoid to quinoid, which has straighter chains that encourage ionic current and current flow paths resulting in the impedance drop. After ~80%RH, the absorption of water molecules by the PSS chains reached a saturation point then the impedance modulus started decreasing more softly since this threshold is defined as a maximum detection limit [11,70]. PEDOT:PSS combined with high conformability and biocompatibility substrate appreciably promotes device integration with a wide range of functional biosensing applications [69].

III. Experimental Section

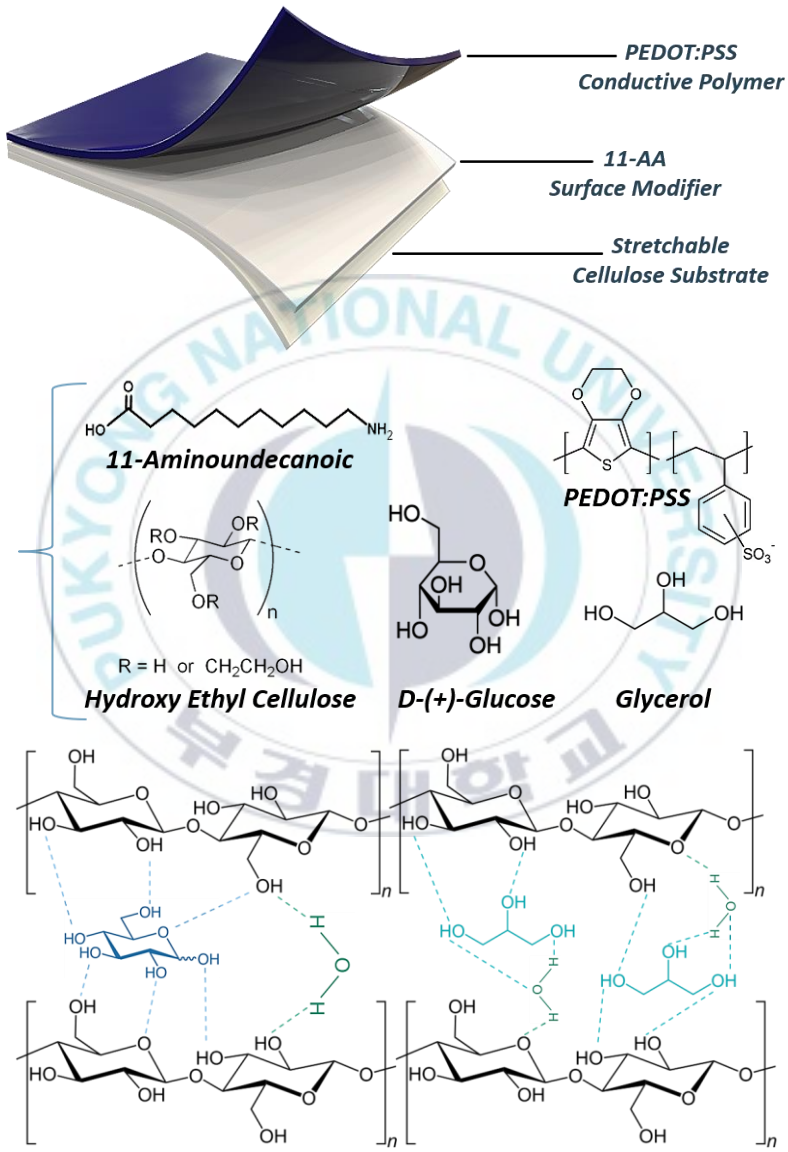

Figure 18. Chemical structure of cellulose/PEDOT: PSS

Materials: Hydroxyethyl Cellulose, Glycerol (MW : 92.09 g/mol), D-(+)-Glucose (MW: 180.16 g/mol) was purchased from Sigma Aldrich. Poly(3,4-ethylenedioxythiophene):poly(styrene sulfonate) (PEDOT:PSS, Clevios PH1000) was purchased from Heraeus. 11-aminoundecanoicacid (11-AA) powder was purchased from Sigma Aldrich.

Preparation of stretchable cellulose substrate: 2 gr of HEC powder dissolved in 100 mL water at room temperature for 60 minutes. Then dissolve the glycerol at a ratio of 10 v/v% for 30 minutes. After 30 minutes, change the temperature to 80°C for 4 hours. Next, stir and dissolve the D-glucose in a ratio of 3 wt% for 10 minutes to increase its stretchability. Put it in a vacuum desiccator until the bubbles disappear then pour it into a petri glass and dried in the oven 80ºC for 12 hours.

Preparation of PEDOT:PSS solution: 10 mL of PH1000 sonicated for 8 minutes then added 0.6 mL of ethylene glycol and 10 uL of non-ionic surfactant FS-31. Then filtered using 0.45 um PVDF

Fabrication of Stretchable Cellulose/PEDOT:PSS film: Cellulose films were treated with UV-plasma for 15 minutes. Then the 11-aminoundecanoic acid spin-coated at a speed of 1000 rpm/30s and annealed at 100ºC for 10 minutes. After that, spin coating PEDOT:PSS at a speed of 2000 rpm/30s and annealed at 120ºC for 10 minutes. The PEDOT:PSS coating repeated three times to generate a better conductivity layer.

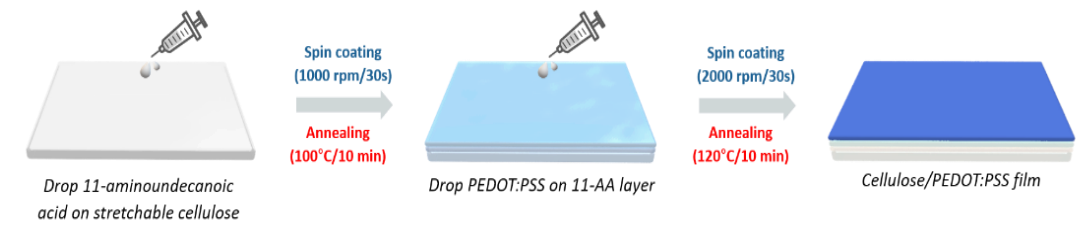

Figure 19. 11-AA and PEDOT:PSS depositions

Characterization: The sheet resistance of cellulose/PEDOT:PSS films measured by the van der Pauw method using a source-meter unit instrument (Keithley 2401). The transmittance measured by the UV-Vis Spectrophotometer (UV-2600). The physical and chemical surface conditions analyzed using Scanning Electron Microscopy and X-Ray Photoelectron Spectroscopy. Characterization of weight degradation due to the temperature increase using Thermogravimetric Analysis. For human-skin sensors, cellulose film wired from our body skin to a source meter unit instrument (Keithley 2401). The temperature sensor is also analyzed using a Keithley 2401 with a Fluke TiS45 to detect temperature distribution.

IV. Results and Discussion

1. Stretchability and Transmittance of Cellulose Substrate

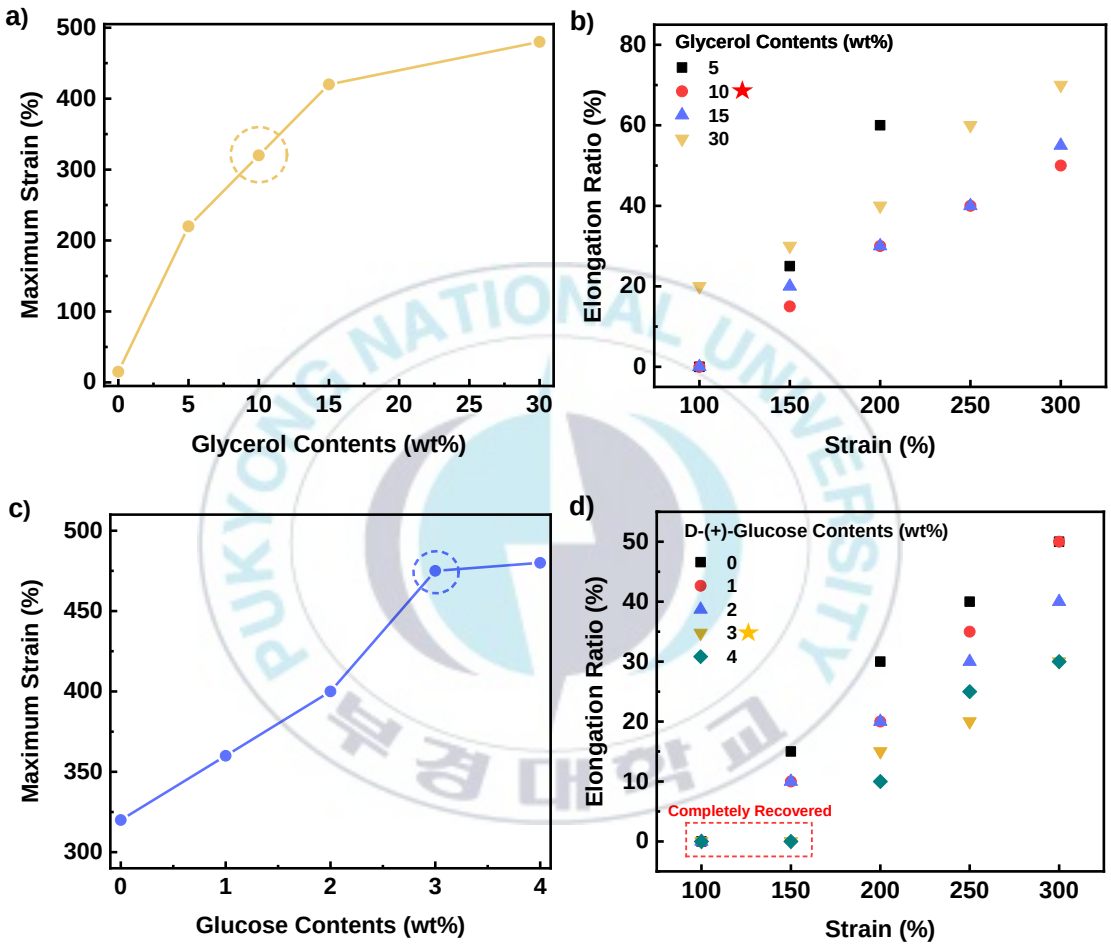

Figure 20. Optimized stretchability of cellulose substrate.

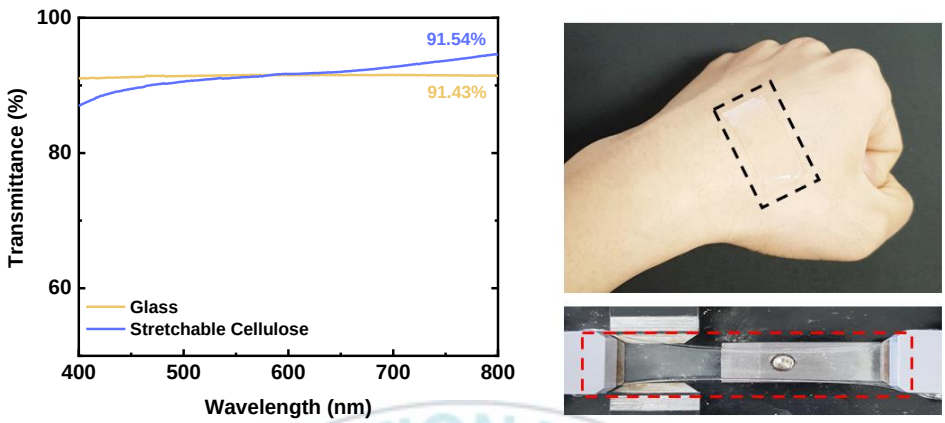

Figure 21. Skin-attachable and transmittance of cellulose substrate.

We have successfully designed stretchable cellulose attributed to glycerol and glucose as plasticizers, resulting in cellulose with a stretchability of ~450%. **Figure 20a and b** depicts the extension of stretchability as glycerol increases. However, higher glycerol contents compose the film more watery, glutinous, and ineligible strain recovery. The elongation ratio calculated by $(\Delta L/L_0) \times 100\%$ to characterize the ability of cellulose to recover back after being strained up to 300%. Hence, a 10wt% glycerol is appropriately considered over several factors. **Figure 20c and d** displays that increasing the glucose contents extends its stretchability up to ~450% and has a qualified strain recovery at 3-4wt%. Plasticizer molecules interact between cellulose chains via hydrogen bonds (O-H), which have the dynamic behavior of supramolecular chains, boost bond mobility and increase the free volume[17,18]. **Figure 21** performs a stretchable cellulose film with excellent skin conformability and a high transmittance.

2. Doping of PEDOT:PSS Solution

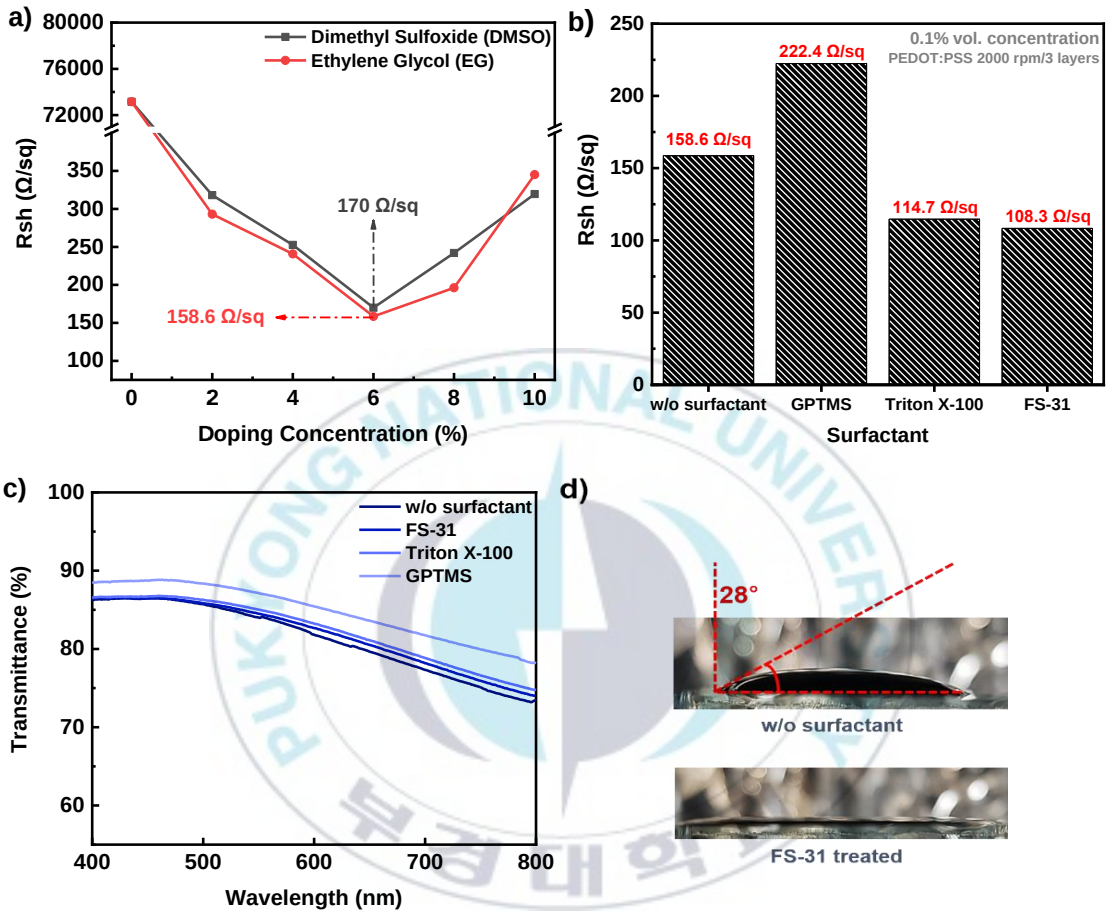

Figure 22. a) Resistance trends to the concentration reducing agents. **b)** Effect of surfactant type in resistance and **c)** Transmittance. **d)** Reduction of contact angle.

Figure 22a depicts the resistance trend as a result of doping concentration. EG improved connectivity between PEDOT grain in the film by reduce coulombic interaction of PEDOT:PSS which lowered the energy barrier for inter grain hopping and promoted the charge transfer. **Figure 22b** reports the resistance value to the type

of surfactant. **Figure 22c** shows the transmittance values of surfactant effects up to 82%. Non-ionic fluorosurfactant FS-31 has excellent conductivity at a concentration of 0.1 %vol by improving coating quality and reduce surface tension.

3. Electro-Mechanical Properties

3.1 Transmittance and Strain-Resistance

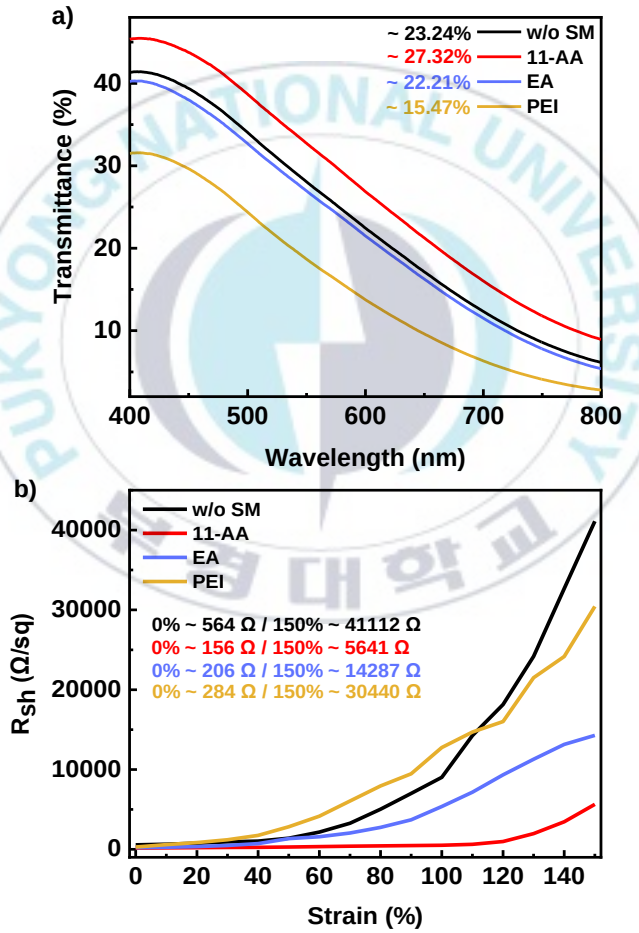

Figure 23. a) Transmittance and **b)** Resistance trends of cellulose/PEDOT:PSS with 11-AA, EA and PEI as surface modifier.

We investigated several types of surface modifiers including 11-aminoundecanoic acid (11-AA), ethanolamine (EA), and polyethylenimine (PEI). Each surface modifier has a different chemical structure, surface energy, and interface interactions. **Figure 23a)** characterizes the difference in transmittance where the 11-AA surface modifier has the highest value compared to EA and PEI. **Figure 23b)** illustrates the resistance when subjected to a strain force of up to 150%. Surface modifier 11-AA has the lowest initial sheet resistance of 156 Ω/sq and expresses the declivous trend. In comparison, the use of surface modifiers 11-AA, EA, PEI, and without surface modifiers led to resistance increases when stretched up to 150% which are 5641 Ω/sq, 14287 Ω/sq, 30440 Ω /sq, and 41112 Ω/sq respectively. The 11-AA interface coating creates a strong chemical bond between the cellulose and the PEDOT: PSS. The adhesiveness is strengthened by the contact layer and allowing for proper PEDOT: PSS deposition. Sulfur (S) molecules of PEDOT:PSS (SO_3^-) can form ionic and covalent bonds with positively charged NH_3^+. Then, negatively charged COOH in 11-AA well-contacted with hydrogen-rich bond in cellulose substrate. Furthermore, the hydroxyl group of cellulose and the 11-AA are linked, resulting in an effective connection between PEDOT: PSS and stretchable cellulose. The presence of a surface modifier as a bond bridge enhances the electrical and mechanical properties of cellulose/PEDOT:PSS composite.

3.2 Electromechanical Stability

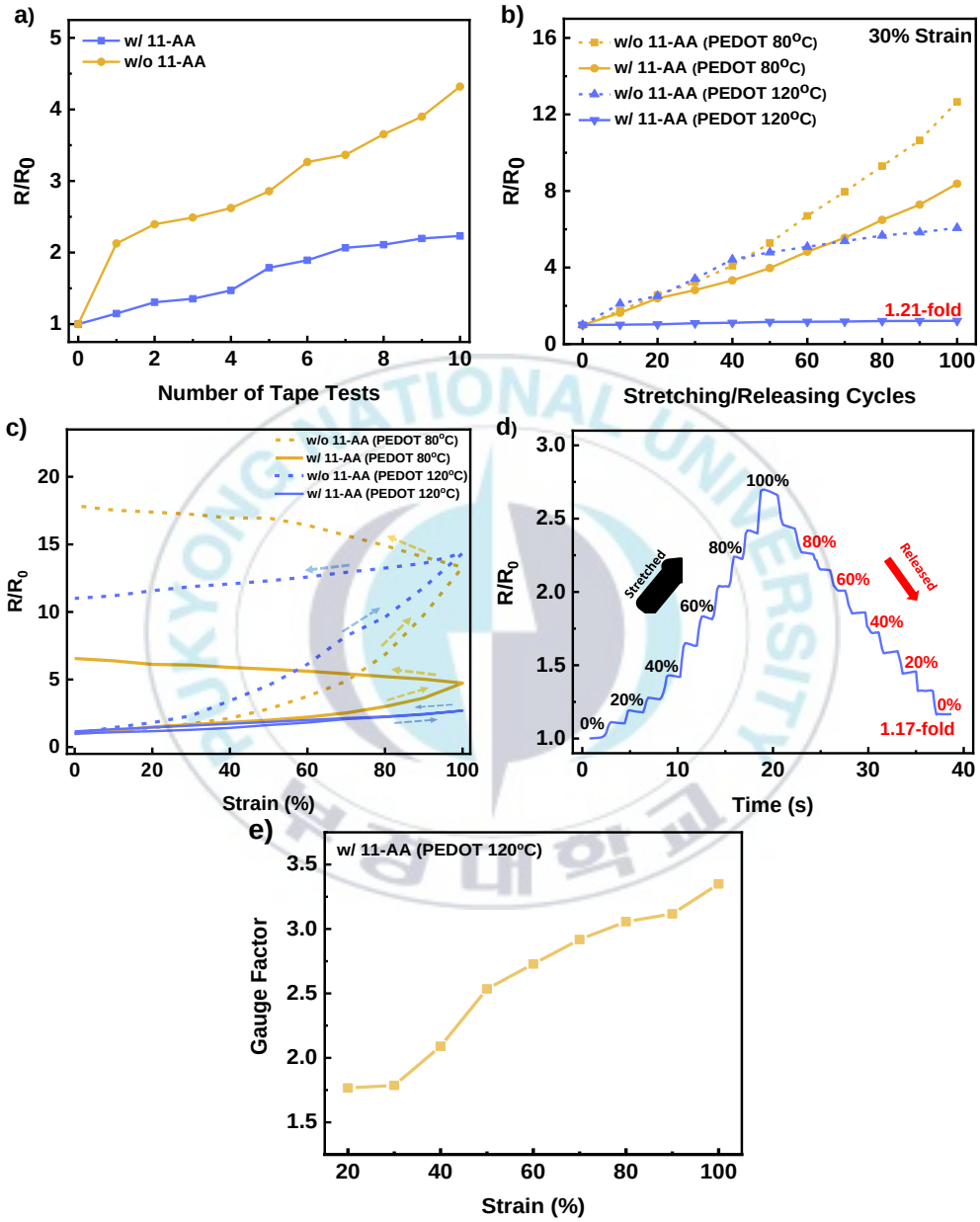

Figure 24. a) Tape test, **b)** Stretching/Releasing Cycles, **c)** Strain-Release test, **d)** Drift characteristic and **e)** Gauge Factor

Figure 24a depicts the resistance changes of cellulose/PEDOT: PSS film treated and untreated 11-AA after a 10 cycles tape test. The presence of 11-AA demonstrates that physical adhesivity performance is superior to untreated 11-AA. **Figure 24b** shows the resistance increase after 100 cycles of stretching and releasing. The annealing temperature has an impact on stretchability as well. At 120°C annealing, treated 11-AA performs 1.21-fold, while untreated 11-AA increased 6.07-fold. The annealing temperature 80ºC with untreated 11-AA and treated 11-AA experienced resistance increases of up to 12.65-fold and 8.38-fold, respectively. Furthermore, in **Figure 24c** the strained-reversed test was performed on strains from 0% - 100% - 0%. The cellulose/PEDOT film with 11-AA treatment at an annealing temperature of 120ºC has a narrower hysteresis line that characterizes the stability enhancement. The annealing temperature controls shrinkage susceptibility and layer thickness[72,73]. **Figure 24d** demonstrates the sensor's drift characteristic over ascending and descending stepping strains from 0% to 100% , resulting no discernible changes in resistance. **Figure 24e** shows the sensitivity between resistance and strain that evaluated by the gauge factor. It can be seen that the sensor becomes more responsive as it elongates. Reversible disconnection-reconnection of cracks endows the strain sensor with high sensitivity and repeatability.

4. Surface Performance

4.1 Lighting Test

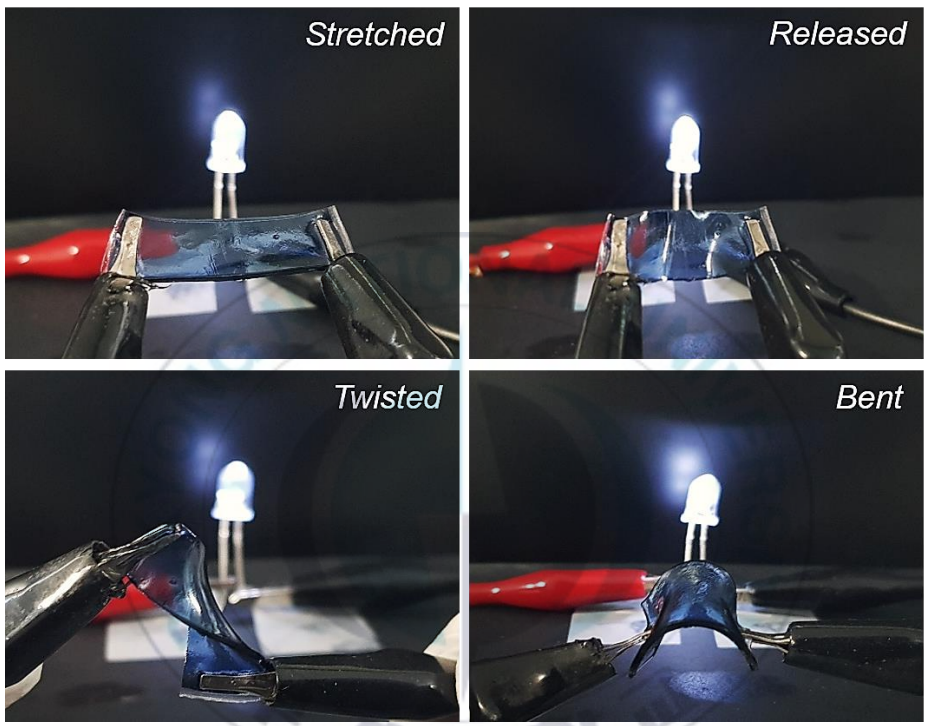

Figure 25. Conductivity of cellulose/PEDOT:PSS to keep the light bulb turning on.

Figure 25 captures the conductivity of stretchable cellulose/PEDOT: PSS, which is sufficient to conduct current flow and keep a light bulb turned on when powered by a 1.5 V AAA size battery. Proving that PEDOT: PSS is uniformly distributed to smoothen out the moving of electrons and the circuit directs an electric current well.

4.2 Scanning Electron Microscopy

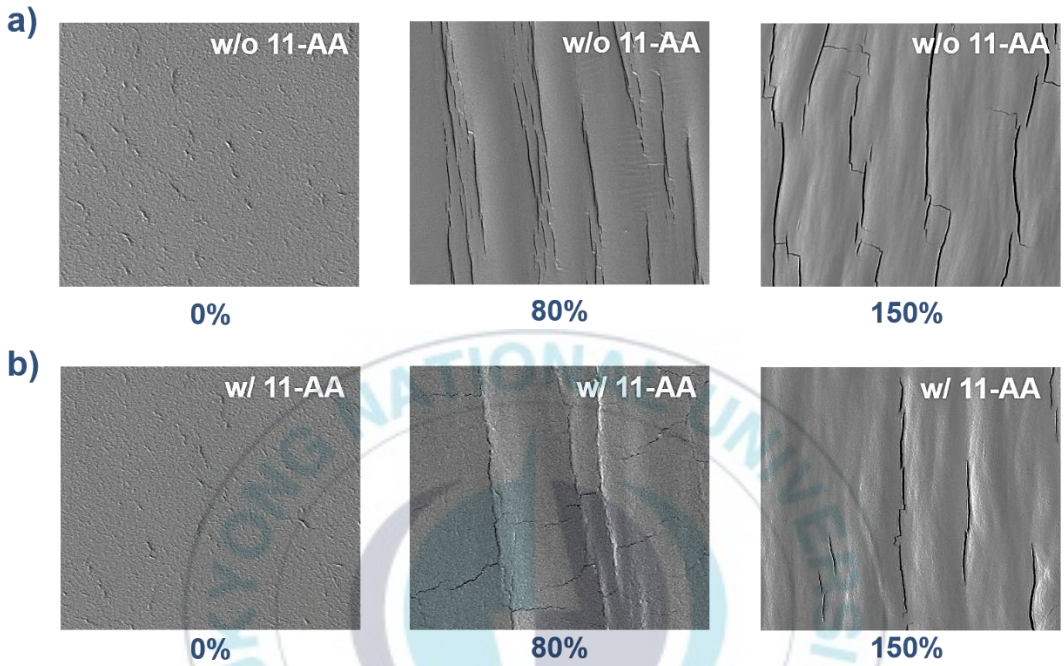

Figure 26. SEM image of cellulose/PEDOT:PSS before and after stretching up to 150% **a)** untreated 11-AA and **b)** treated 11-AA

Figure 26 captures the surface morphology of treated and untreated 11-AA after 150% stretching. In **Figure 26a**, the untreated 11-AA of cellulose/PEDOT: PSS generated significantly more cracks after stretching than the treated 11-AA film. Cracks propagate more easily when subjected to tensile forces due to inhomogeneous PEDOT: PSS distribution and the inadequacy of reinforcing bonds on untreated 11-AA. Conversely in **Figure 26b**, the presence of an interface 11-AA layer in the PEDOT offers crack resistance on the PEDOT: PSS coating after 150 % stretching.

4.3 X-Ray Photoelectron Spectroscopy

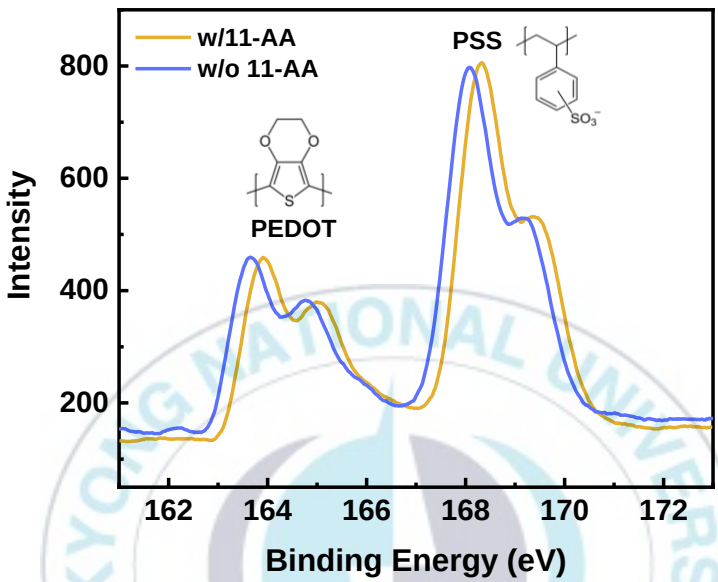

Figure 27. Surface analysis of cellulose/PEDOT:PSS by XPS

Figure 27 presents the distribution of elemental sulfur (S 2p) in PEDOT: PSS. The doublet peaks between 163eV and 165eV represent the existence of sulfur atoms in thiophene groups (PEDOT), while at binding energy 167eV – 171eV there is a distribution of sulphonate groups by counterions (PSS). The chemical shift occurred to higher binding energy that corresponds to higher oxidation state and lowering the PSS-to-PEDOT ratio from 1.81 : 1 to 1.75 : 1. The 11-AA treatment strengthens the adhesion between substrate surfaces and PEDOT: PSS to improve electrical and surface properties.

5. Hydro and Thermal Degradation

5.1 Water-Transience

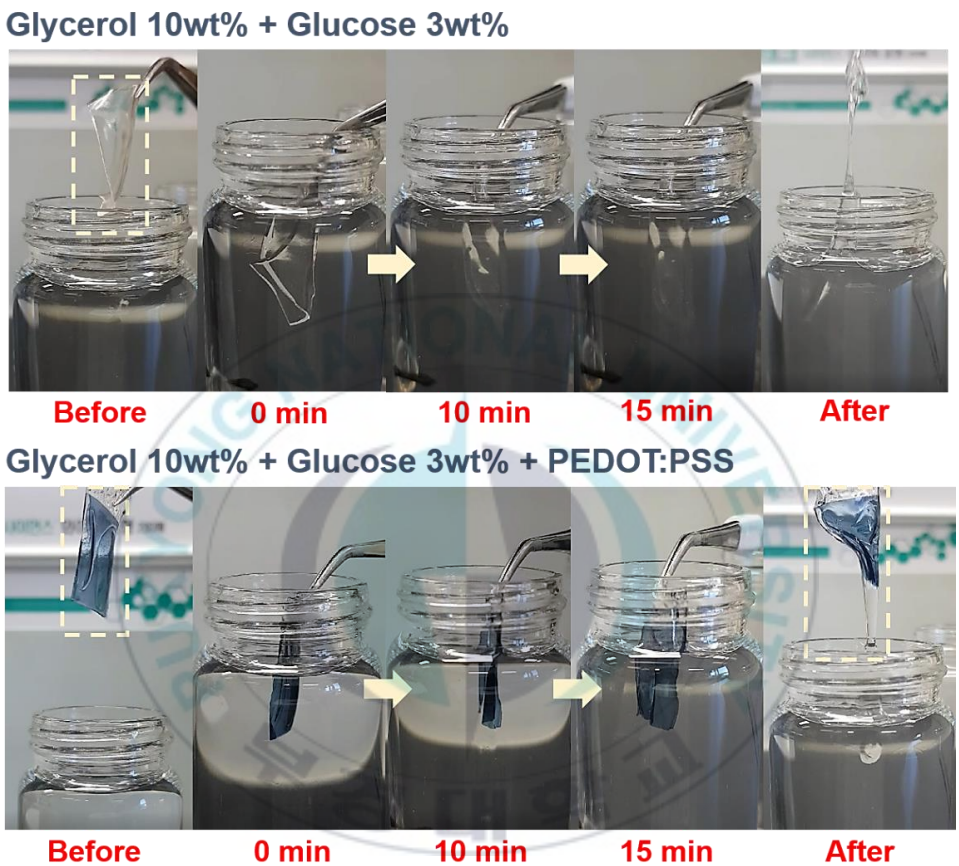

Figure 28. Photograph of water-transience process

Figure 28 perform all samples transform transiently within the first 15 minutes. Water molecules interact with glycerol at the outer layer to replace and the glycerol dissolves, which promotes the binding of water molecules to the HEC. The same process is followed from the outer to the inner layers, with GHEC being entirely dissolved at the end. Furthermore, because of its high affinity and hydrophilicity,

cellulose effectively interacts with water molecules. The smallness of water molecule enables them to react easily with cellulose chain and by creating hydrogen bond through capillary forces. Some of the hydrogen-bonding networks in the cellulose chain will disappear, and compensated by novel hydrogen from water molecules[74,75].

5.2 Thermal Degradation

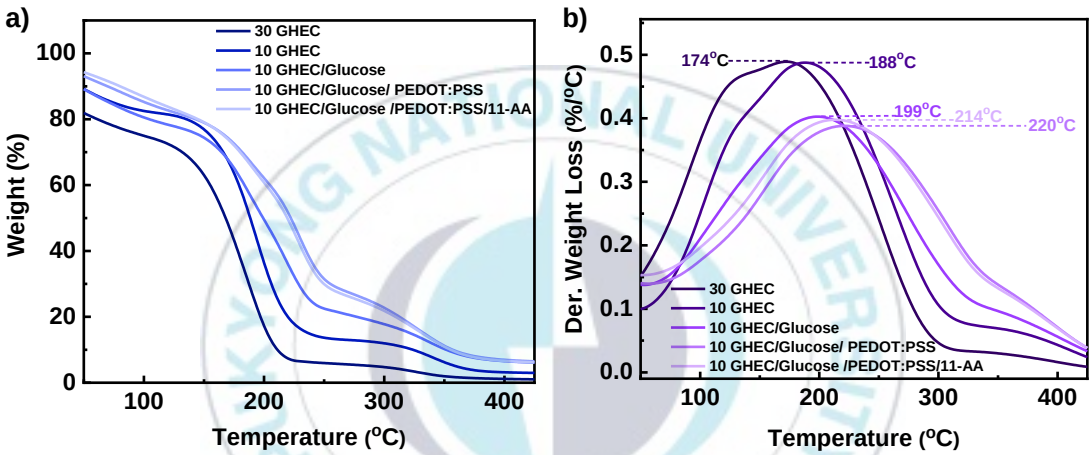

Figure 29. a) Thermal degradation of cellulose/PEDOT:PSS by TGA analysis **b)** First derivative of weight loss

The T-G curve describes the weight loss as the temperature rises to 400°C. The reduction of glycerol and increasing glucose content shifted the optimum degradation temperature (ODT) to a higher temperature. 10 wt% glycerol and PEDOT: PSS slow down the thermal degradation by inhibiting the heat transfer at initial stage and has higher ODT value, reaching 214°C and 220°C. Then it was completely depolymerized at ~350°C. As a result, the safe detection limit for temperature sensor is 120°C.

6. Multifunctional Sensor Applications

6.1 Human Skin Sensor

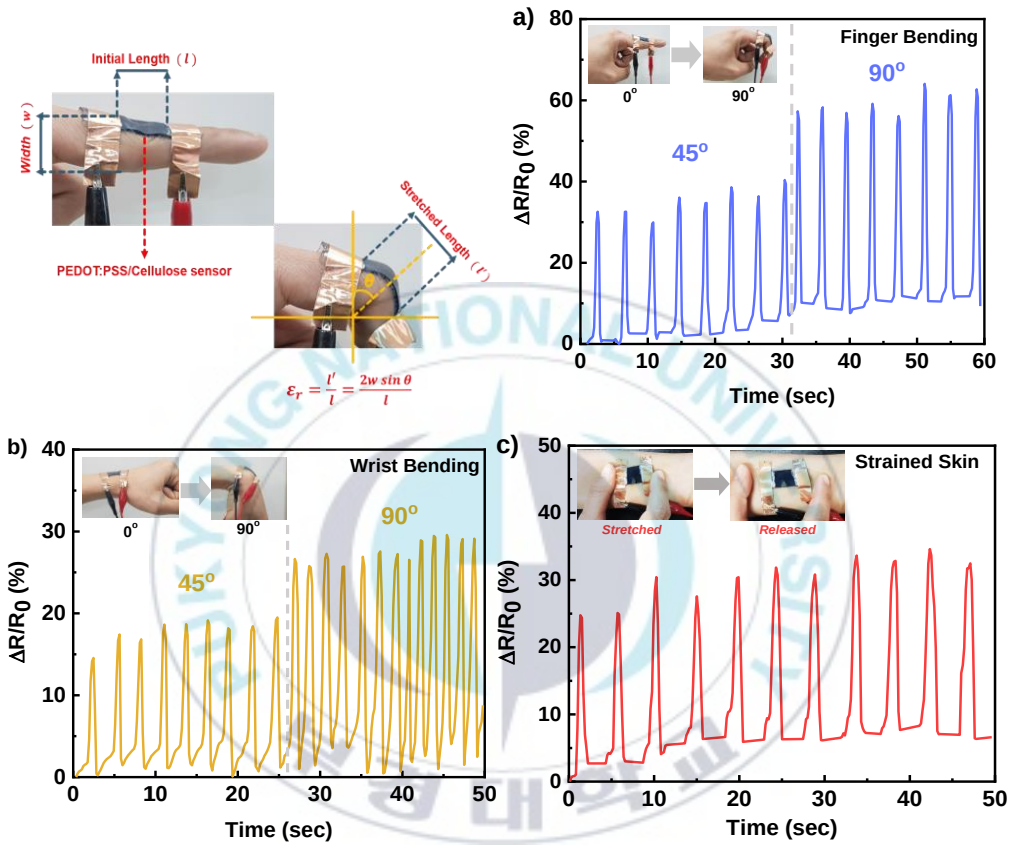

Figure 30. Human skin sensor attached on **a)** finger, **b)** wrist and **c)** hand's skin to respond large motion such as bent and wrinkled.

We integrate cellulose/PEDOT: PSS sensor into several body parts, including the fingers, wrist, skin, diaphragm, and larynx, to respond the movements and vibrations. **Figures 30a** and **30b** depict the change in relative resistance ($\Delta R/R_0$) attached to fingers and wrists that bent 45°/90° and then straightened (0°).

The ($\Delta R/R_0$) confirm a consistent response at an average of 30% (45°) and 60% (90°) finger bends. Furthermore, the ($\Delta R/R_0$) of wrist flexion was on average 18% (45°) and 26% (90°). **Figure 30c** depicts the change in relative resistance triggered by stretch/release forces on the skin's surface. Because cellulose/PEDOT: PSS has high conformability properties, skin wrinkles cause an average change in resistance of up to 30% when wrinkled.

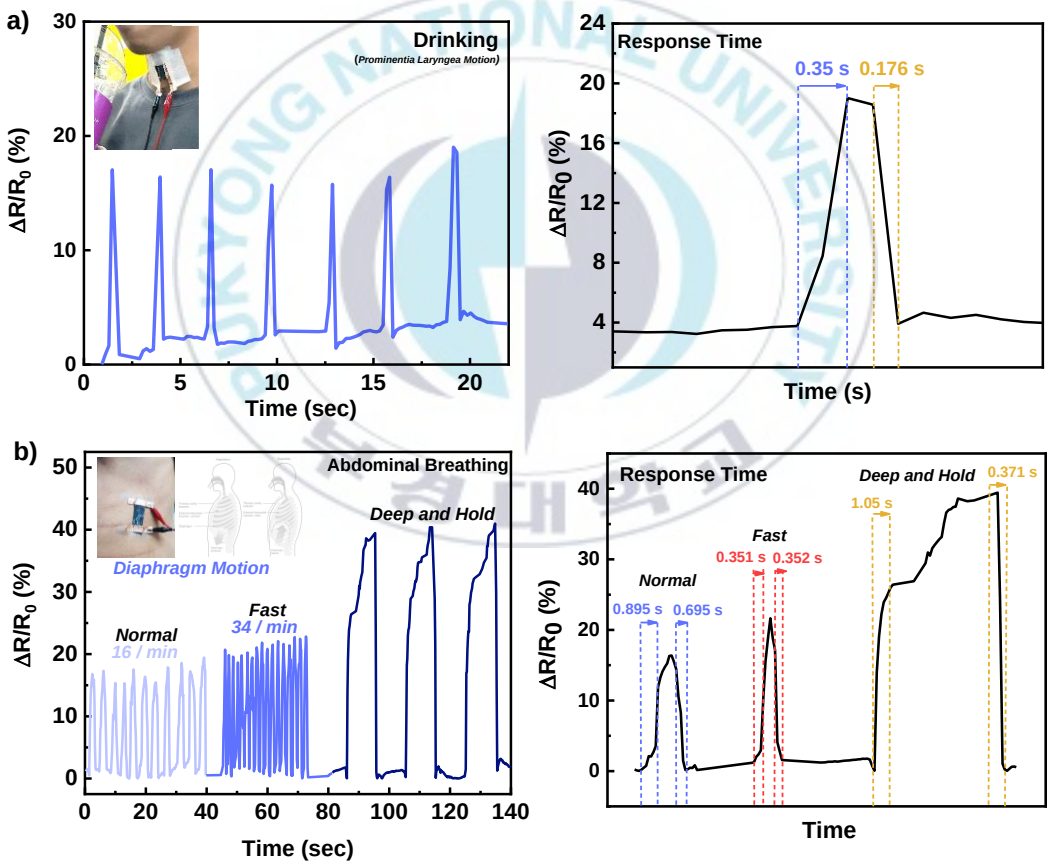

Figure 31. Human skin sensor attached on **a)** throat and **b)** diaphragm to respond vibration

Figure 31a depicts the relative change in resistance provoked by laryngeal activity when drinking water. The sensor is mounted to the throat and monitors a real-time vibration with an ($\Delta R/R_0$) 15% on averages that shows response time of 0.35 sec then a recovery time of 0.176 sec after swallowing. **Figure 31b** also captures the change in resistance intensity when breathing properly, rapidly, and deeply which are able to distinguish the intensity of the vibration and the response/recovery time that occurs during the inhalation and exhalation process. Contraction and relaxation of the diaphragm muscle force a change in relative resistance of 16% (normal breathing), 20% with rapid lines (fast breathing), and 40% with different patterns of deep breathing and holding for a few seconds. Deformation increases the tunnel distance and the destruction of conductive path leads to an increase of resistance during stretching. Conversely, return to the initial resistance to decrease the tunnel distance and recover the conductivity pathway during the retraction process, thereby resulting in decreased resistance. This outstanding sensitivity indicates that it has great potential as a healthcare monitoring function, such as detecting the intensity of ingesting/coughing, respiratory and physiological activities.

6.2 Temperature Sensor

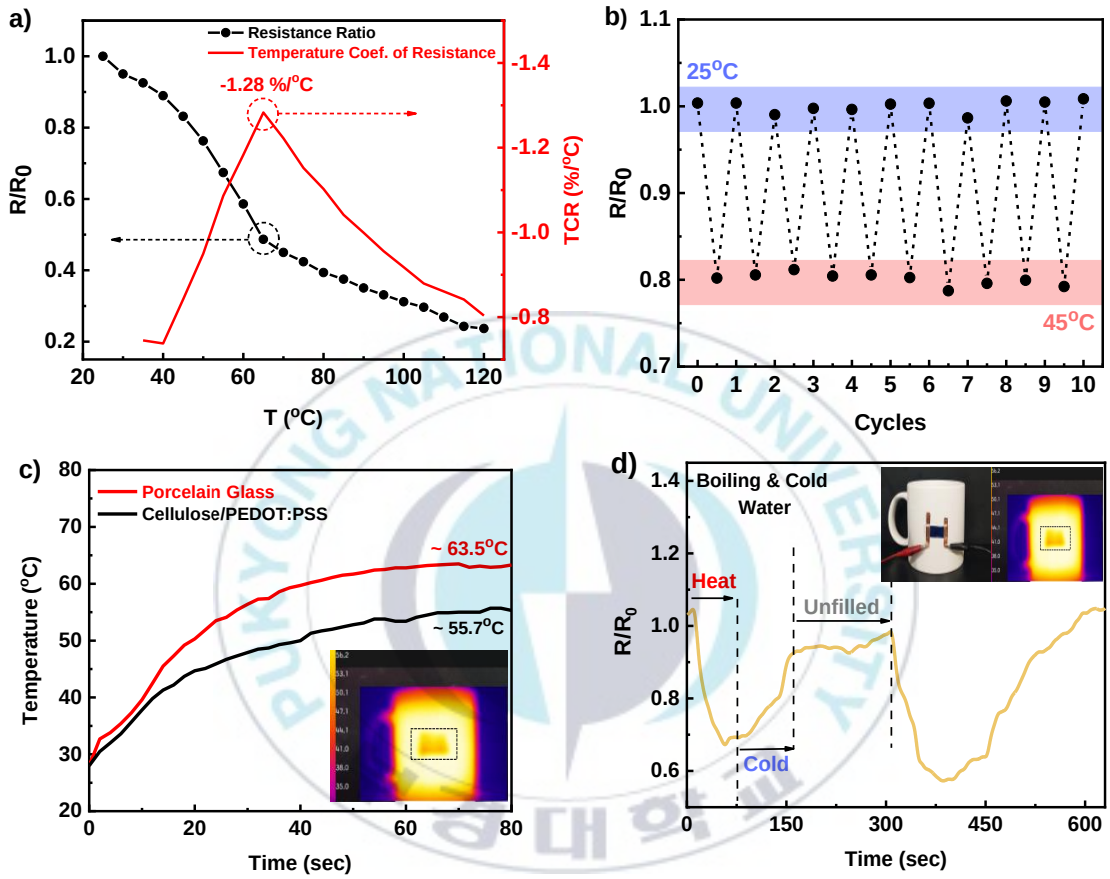

Figure 32. a) T-R function performance as temperature sensor and temperature coefficient of resistance (TCR). **b)** Stability test by temperature cycles. **c)** Heat distribution on the mug wall and PEDOT:PSS/Cellulose. **d)** Resistance fluctuation when induced by cold and boiled water.

Figure 32a clearly demonstrates that the resistance downwards when heated up to 120°C and describes the temperature coefficient of resistance (TCR = α) with the following formula,

$$R_t = R_i\,[1 + \alpha\,(T - T_0)] \quad (7)$$

$$\alpha = -\left(\frac{R_i - R_t}{R_i} \times \Delta T^{-1}\right) \times 100\% \quad (8)$$

$(R_i\text{-}R_t)/R_i$ symbolizes the difference in resistance decrease as temperature (T) increases. The maximum TCR value for cellulose/PEDOT: PSS at 65ºC is -1.28 %/ºC with averages -0.97%/ºC, indicating that it performs well as a temperature sensor. **Figure 32b** depicts the sensor's stability during cycles of room temperature and 45°C heating. The sensor has excellent stability and reproducibility, sustaining up to 10 cycles and ideal for long-term application. Then, cellulose/PEDOT: PSS applied as a heat sensor on the ceramic glass, which alternately filled with boiling and cold water. **Figure 32d** illustrates the sinusoidal graph of resistance when the mug is filled with boiling and cold water. Thermal energy generates electron-hole pairs and induces thermal excitation from the valence band to the conduction band resulting in a higher charge carrier concentration and increased conductivity. At low temperatures, the number of charge carriers in PEDOT: PSS is insufficient, and when exposed to heat, many lightly bound carriers escape then free to conduct until fully activated.

6.3 Breath Humidity Sensor

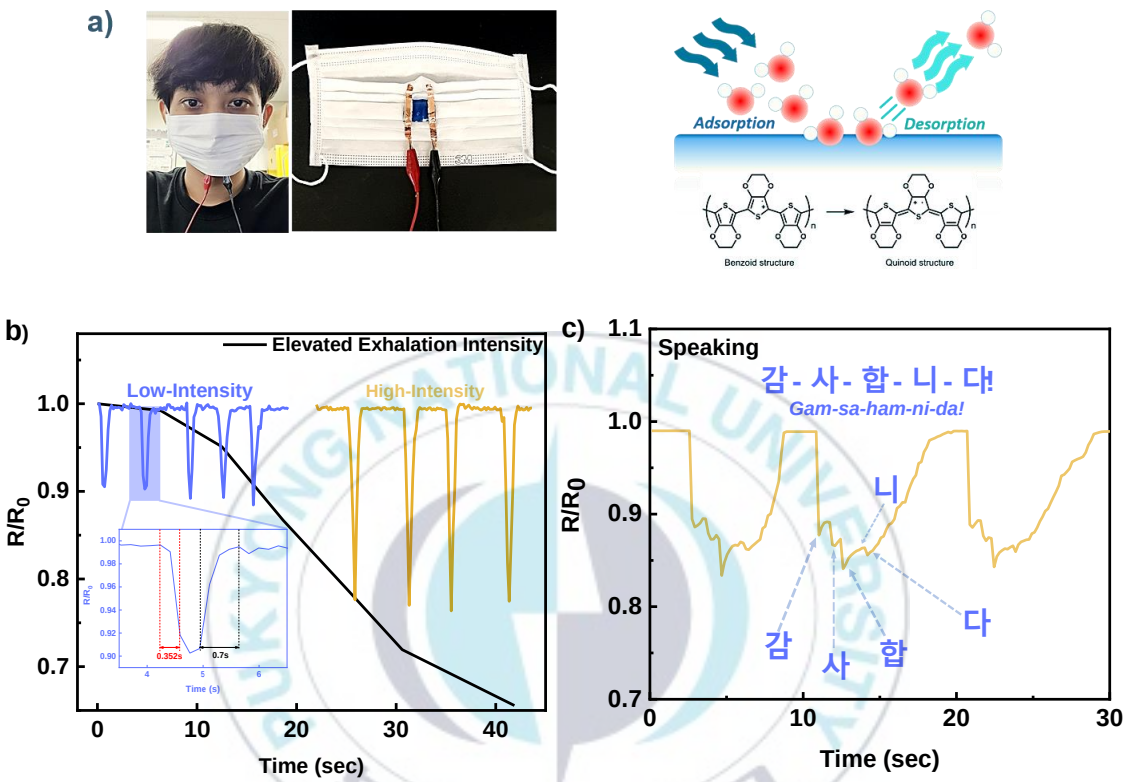

Figure 33. a) Humidity sensor attached on the mask to respond RH level intensity. The sensor sensitivity when applied by **b)** breathing and **c)** speaking

Humidity sensors are a fascinating aspect of PEDOT: PSS that applied to controlling healthcare, medicine, and the environment. **Figure 33a** illustrates how the sensor collects data in resistance changes as a function of humidity level on the respiratory system. **Figure 33b** exhibits the resistance trend when applied to the mask, recording the signal of relative humidity (RH) intensity based on the exhalation

process which leads to electrical resistivity reductions (R/R_0) of up to 0.65-fold. And also illustrates the exhale/inhale system in low-to-high breathing levels. The sensor is able to recognize and distinguish the intensity of water molecules exhaled by the mouth/nose with output resistance changes. Furthermore, **Figure 33c** demonstrates resistance fluctuation when pronouncing the Korean word Gam-Sa-Ham-Ni-Da (means Thankyou in English). The PEDOT: PSS layer detects varied humidity intensities in each syllable, and resistance is reduced. Water adsorption-desorption causes hydroxyl groups (OH) in the PSS chain to dissociate, leading to the formation of coulombic bonds (electrostatic attraction) on cations with sulfonate polyanion groups, increasing positive charge density, bond energy, and mobility in the PEDOT chain. Diffusion of H_2O into PEDOT:PSS drives the protonation of SO_3H^+ groups at the PEDOT:PSS interface terminating in the creation of $H_3O^+ + PSS(SO_3)^-$ [69]. Hydronium ions facilitated the ionic conductions and produces better current flow path within PEDOT chain until RH 80%. Water vapor induces additional doping to the dynamic chains of PEDOT: PSS and transforms a benzoid structure to a straighter quinoid when reacting with water hydrogen bonds thereby facilitating and modulating the ionic conductivity mobility to reduce resistance[11,76–78].

V. Conclusion

In conclusion, this study developed stretchable, biodegradable, and skin-attachable cellulose / PEDOT: PSS for wearable sensor applications. This research improves the cellulose structure with plasticizers such as glycerol and glucose result in a maximum strain of up to 450%. 11-AA is employed as a bonding layer at the interface between stretchable cellulose and PEDOT: PSS to improve electrical, stretchability, and surface properties. Moreover, PEDOT: PSS doped with reducing agent EG to remove insulating PSS counterions, and non-ionic fluorosurfactant FS-31 was used to increase wettability and reduce contact angle so that PEDOT: PSS could be properly deposited. Our sensor has excellent hydro-biodegradability and has a resistance of 156Ω. This study integrated highly conformable cellulose/PEDOT: PSS with human skin to monitor bending, strained skin, and subtle forces of breathing and swallowing/drinking. Besides, cellulose/PEDOT has superior mechanical adsorption/desorption activity that suitable for use as a biological humidity sensor and excellent temperature sensing performance up to a limit of 120^{o}C. The stretchable, biodegradable, and highly sensitive cellulose/PEDOT: PSS films are figured in the development of eco - friendly wearable sensors for monitoring physiological activities, temperature, and biological humidity.

References

1. Kim, Y. H. *et al.* Highly conductive PEDOT:PSS electrode with optimized solvent and thermal post-treatment for ITO-free organic solar cells. *Adv. Funct. Mater.* **21**, 1076–1081 (2011).
2. Bhattacharjee, M., Soni, M., Escobedo, P. & Dahiya, R. PEDOT:PSS Microchannel-Based Highly Sensitive Stretchable Strain Sensor. *Adv. Electron. Mater.* **6**, (2020).
3. Gao, N. *et al.* Application of pedot:Pss and its composites in electrochemical and electronic chemosensors. *Chemosensors* **9**, (2021).
4. Seyedin, M. Z., Razal, J. M., Innis, P. C. & Wallace, G. G. Strain-responsive polyurethane/PEDOT:PSS elastomeric composite fibers with high electrical conductivity. *Adv. Funct. Mater.* **24**, 2957–2966 (2014).
5. Zahid, M., Papadopoulou, E. L., Athanassiou, A. & Bayer, I. S. Strain-responsive mercerized conductive cotton fabrics based on PEDOT:PSS/graphene. *Mater. Des.* **135**, 213–222 (2017).
6. Ramadhan, Z. R. *et al.* Conductive PEDOT:PSS on surface-functionalized chitosan biopolymers for stretchable skin-like electronics. *Org. Electron.* **94**, 106165 (2021).
7. Lim, T. *et al.* Human sweat monitoring using polymer-based fiber. *Sci. Rep.* **9**, 1–8 (2019).
8. Zhang, Y. & Cui, Y. Development of Flexible and Wearable Temperature Sensors Based on PEDOT:PSS. *IEEE Trans. Electron Devices* **66**, 3129–3133 (2019).
9. Wang, Y. F. *et al.* Fully Printed PEDOT:PSS-based Temperature Sensor with High Humidity Stability for Wireless Healthcare Monitoring. *Sci. Rep.*

10, 1–8 (2020).

10. Lee, J. W. *et al.* PEDOT:PSS-based temperature-detection thread for wearable devices. *Sensors (Switzerland)* **18**, 2–9 (2018).
11. Hassan, G., Sajid, M. & Choi, C. Highly Sensitive and Full Range Detectable Humidity Sensor using PEDOT:PSS, Methyl Red and Graphene Oxide Materials. *Sci. Rep.* **9**, 1–10 (2019).
12. Takei, A. *et al.* Stretchable and durable Parylene/PEDOT:PSS/Parylene multi-layer induced by plastic deformation for stretchable device using functionalized PDMS. *AIP Adv.* **10**, (2020).
13. Luo, R., Li, H., Du, B., Zhou, S. & Zhu, Y. A simple strategy for high stretchable, flexible and conductive polymer films based on PEDOT:PSS-PDMS blends. *Org. Electron.* **76**, 105451 (2020).
14. Beccatelli, M. *et al.* All-Polymeric Pressure Sensors Based on PEDOT:PSS-Modified Polyurethane Foam. *ACS Appl. Polym. Mater.* **3**, 1563–1572 (2021).
15. Irimia-Vladu, M., Głowacki, E. D., Voss, G., Bauer, S. & Sariciftci, N. S. Green and biodegradable electronics. *Mater. Today* **15**, 340–346 (2012).
16. Sehaqui, H., Morimune, S., Nishino, T. & Berglund, L. A. Stretchable and strong cellulose nanopaper structures based on polymer-coated nanofiber networks: An alternative to nonwoven porous membranes from electrospinning. *Biomacromolecules* **13**, 3661–3667 (2012).
17. Lim, D. B. K. & Gong, H. Highly stretchable and transparent films based on cellulose. *Carbohydr. Polym.* **201**, 446–453 (2018).
18. Hao, M. *et al.* Stretchable, self-healing, transient macromolecular elastomeric gel for wearable electronics. *Microsystems Nanoeng.* **5**, (2019).
19. Huang, S. *et al.* Facile fabrication and characterization of highly stretchable lignin-based hydroxyethyl cellulose self-healing hydrogel. *Carbohydr.*

Polym. **223**, (2019).

20. Vosgueritchian, M., Lipomi, D. J. & Bao, Z. Highly conductive and transparent PEDOT:PSS films with a fluorosurfactant for stretchable and flexible transparent electrodes. *Adv. Funct. Mater.* **22**, 421–428 (2012).
21. Pathak, C. S., Singh, J. P. & Singh, R. Effect of dimethyl sulfoxide on the electrical properties of PEDOT:PSS/n-Si heterojunction diodes. *Curr. Appl. Phys.* **15**, 528–534 (2015).
22. Yi, M. *et al.* Modification of a PEDOT:PSS hole transport layer for printed polymer solar cells. *Sol. Energy Mater. Sol. Cells* **153**, 117–123 (2016).
23. Mahato, S., Gerling, L. G., Voz, C., Alcubilla, R. & Puigdollers, J. PEDOT:PSS as an Alternative Hole Selective Contact for ITO-Free Hybrid Crystalline Silicon Solar Cell. *IEEE J. Photovoltaics* **6**, 934–939 (2016).
24. Entifar, S. A. N. *et al.* Simultaneously enhanced optical, electrical, and mechanical properties of highly stretchable transparent silver nanowire electrodes using organic surface modifier. *Sci. Technol. Adv. Mater.* **20**, 116–123 (2019).
25. Wu, W. Stretchable electronics: functional materials, fabrication strategies and applications. *Sci. Technol. Adv. Mater.* **20**, 187–224 (2019).
26. Rogers, J. A., Someya, T. & Huang, Y. Materials and mechanics for stretchable electronics. *Science (80-.).* **327**, 1603–1607 (2010).
27. Kim, J. *et al.* Stretchable silicon nanoribbon electronics for skin prosthesis. *Nat. Commun.* **5**, (2014).
28. Wang, X. & Liu, J. Recent advancements in liquid metal flexible printed electronics: Properties, technologies, and applications. *Micromachines* **7**, (2016).
29. Park, Y. L., Chen, B. R. & Wood, R. J. Design and fabrication of soft artificial skin using embedded microchannels and liquid conductors. *IEEE*

Sens. J. **12**, 2711–2718 (2012).

30. Liu, Y., Pharr, M. & Salvatore, G. A. Lab-on-Skin: A Review of Flexible and Stretchable Electronics for Wearable Health Monitoring. *ACS Nano* **11**, 9614–9635 (2017).
31. Liu, W. *et al.* Stretchable Lithium-Ion Batteries Enabled by Device-Scaled Wavy Structure and Elastic-Sticky Separator. *Adv. Energy Mater.* **7**, 1–6 (2017).
32. Song, J. *et al.* Mechanics of noncoplanar mesh design for stretchable electronic circuits. *J. Appl. Phys.* **105**, 2–7 (2009).
33. Collins, G. P. Kirigami and technology cut a fine figure, together. *Proc. Natl. Acad. Sci. U. S. A.* **113**, 240–241 (2016).
34. Almuslem, A. S., Shaikh, S. F. & Hussain, M. M. Flexible and Stretchable Electronics for Harsh-Environmental Applications. *Adv. Mater. Technol.* **4**, 1–18 (2019).
35. Irimia-Vladu, M. 'Green' electronics: Biodegradable and biocompatible materials and devices for sustainable future. *Chem. Soc. Rev.* **43**, 588–610 (2014).
36. Zoeteman, B. C. J., Krikke, H. R. & Venselaar, J. Handling WEEE waste Hows: On the effectiveness of producer responsibility in a globalizing world. *Int. J. Adv. Manuf. Technol.* **47**, 415–436 (2010).
37. Awasthi, A. K., Zeng, X. & Li, J. Environmental pollution of electronic waste recycling in India: A critical review. *Environ. Pollut.* **211**, 259–270 (2016).
38. Kaltenbrunner, M. *et al.* Ultrathin and lightweight organic solar cells with high flexibility. *Nat. Commun.* **3**, (2012).
39. Jung, Y. H. *et al.* High-performance green flexible electronics based on biodegradable cellulose nanofibril paper. *Nat. Commun.* **6**, (2015).

40. Gao, K. *et al.* Cellulose nanofiber-graphene all solid-state flexible supercapacitors. *J. Mater. Chem. A* **1**, 63–67 (2013).
41. Huang, J. *et al.* Highly transparent and flexible nanopaper transistors. *ACS Nano* **7**, 2106–2113 (2013).
42. Nagashima, K. *et al.* Cellulose nanofiber paper as an ultra flexible nonvolatile memory. *Sci. Rep.* **4**, 1–7 (2014).
43. Spain, E. & Venkatanarayanan, A. *Review of Physical Principles of Sensing and Types of Sensing Materials*. *Comprehensive Materials Processing* vol. 13 (Elsevier, 2014).
44. Bezugly, V. Wavefunction-based method for excited-state electron correlations in periodic systems - application to polymers. (2004).
45. Zeng, Q. *et al.* A new disubstituted polyacetylene for the detection of a-amino acids. *Macromol. Rapid Commun.* **30**, 170–175 (2009).
46. Harlin, A. & Ferenets, M. Introduction to conductive materials. *Intell. Text. Cloth.* 217–238 (2006) doi:10.1533/9781845691622.3.217.
47. Dhand, C., Das, M., Datta, M. & Malhotra, B. D. Recent advances in polyaniline based biosensors. *Biosens. Bioelectron.* **26**, 2811–2821 (2011).
48. Boddula, R. & Srinivasan, P. Emeraldine Base Form of Polyaniline Nanofibers as New, Economical, Green, and Efficient Catalyst for Synthesis of Z -Aldoximes . *J. Catal.* **2014**, 1–6 (2014).
49. Stafström, S. *et al.* Polaron lattice in highly conducting polyaniline: Theoretical and optical studies. *Phys. Rev. Lett.* **59**, 1464–1467 (1987).
50. Mzenda, V. M., Goodman, S. A. & Auret, F. D. Conduction models in polyaniline: The effect of temperature on the current-voltage properties of polyaniline over the temperature range 30 < T(K) < 300. *Synth. Met.* **127**, 285–289 (2002).
51. Liu, H., Ge, J., Ma, E. & Yang, L. *Advanced biomaterials for biosensor and*

theranostics. *Biomaterials in Translational Medicine: A Biomaterials Approach* (Elsevier Inc., 2018). doi:10.1016/B978-0-12-813477-1.00010-4.

52. Qu, L., Xia, S., Bian, C., Sun, J. & Han, J. A micro-potentiometric hemoglobin immunosensor based on electropolymerized polypyrrole-gold nanoparticles composite. *Biosens. Bioelectron.* **24**, 3419–3424 (2009).

53. Liang, Y. & Goh, J. C.-H. Polypyrrole-Incorporated Conducting Constructs for Tissue Engineering Applications: A Review. *Bioelectricity* **2**, 101–119 (2020).

54. Arakawa, C. K. & DeForest, C. A. *Polymer Design and Development*. *Biology and Engineering of Stem Cell Niches* (Elsevier Inc., 2017). doi:10.1016/B978-0-12-802734-9.00019-6.

55. Kwon, S., Han, S., Ihm, D., Kim, E. & Kim, J. Preparation and characterization of conductive polymer nano-films. *Mol. Cryst. Liq. Cryst.* **425**, 77–83 (2004).

56. Quirós-Solano, W. F., Gaio, N., Silvestri, C., Pandraud, G. & Sarro, P. M. PEDOT:PSS: A Conductive and Flexible Polymer for Sensor Integration in Organ-on-Chip Platforms. *Procedia Eng.* **168**, 1184–1187 (2016).

57. Vaagensmith, B. *et al.* Environmentally Friendly Plasma-Treated PEDOT:PSS as Electrodes for ITO-Free Perovskite Solar Cells. *ACS Appl. Mater. Interfaces* **9**, 35861–35870 (2017).

58. Worfolk, B. J. *et al.* Ultrahigh electrical conductivity in solution-sheared polymeric transparent films. *Proc. Natl. Acad. Sci. U. S. A.* **112**, 14138–14143 (2015).

59. Fan, X. *et al.* PEDOT:PSS for Flexible and Stretchable Electronics: Modifications, Strategies, and Applications. *Adv. Sci.* **6**, (2019).

60. Kim, N. *et al.* Highly conductive PEDOT:PSS nanofibrils induced by solution-processed crystallization. *Adv. Mater.* **26**, 2268–2272 (2014).

61. Yeon, C., Yun, S. J., Kim, J. & Lim, J. W. PEDOT:PSS Films with Greatly Enhanced Conductivity via Nitric Acid Treatment at Room Temperature and Their Application as Pt/TCO-Free Counter Electrodes in Dye-Sensitized Solar Cells. *Adv. Electron. Mater.* **1**, 1–8 (2015).
62. Zein, A. El, Huppé, C. & Cochrane, C. Development of a flexible strain sensor based on PEDOT: PSS for thin film structures. *Sensors (Switzerland)* **17**, 1–14 (2017).
63. Kang, T. K. Inkjet printing of highly sensitive, transparent, flexible linear piezoresistive strain sensors. *Coatings* **11**, 1–8 (2021).
64. Mathew, X. Solar cells & solar energy materials: Cancun 2003. *Sol. Energy Mater. Sol. Cells* **82**, 1–2 (2004).
65. Vuorinen, T., Niittynen, J., Kankkunen, T., Kraft, T. M. & Mäntysalo, M. Inkjet-printed graphene/PEDOT:PSS temperature sensors on a skin-conformable polyurethane substrate. *Sci. Rep.* **6**, 1–8 (2016).
66. Yu, Y., Peng, S., Blanloeuil, P., Wu, S. & Wang, C. H. Wearable Temperature Sensors with Enhanced Sensitivity by Engineering Microcrack Morphology in PEDOT:PSS-PDMS Sensors. *ACS Appl. Mater. Interfaces* **12**, 36578–36588 (2020).
67. Yao, X. & Cui, Y. A PEDOT:PSS functionalized capacitive sensor for humidity. *Meas. J. Int. Meas. Confed.* **160**, (2020).
68. Taccola, S. *et al.* Characterization of free-standing PEDOT:PSS/iron oxide nanoparticle composite thin films and application as conformable humidity sensors. *ACS Appl. Mater. Interfaces* **5**, 6324–6332 (2013).
69. Wang, G. *et al.* Fast-response humidity sensor based on laser printing for respiration monitoring. *RSC Adv.* **10**, 8910–8916 (2020).
70. Romero, F. J., Rivadeneyra, A., Becherer, M., Morales, D. P. & Rodríguez, N. Fabrication and characterization of humidity sensors based on graphene

Oxide-PEDOT:PSS composites on a flexible substrate. *Micromachines* **11**, (2020).

71. Ramadhan, Z. R. *et al.* Surface-functionalized silver nanowires on chitosan biopolymers for highly robust and stretchable transparent conducting films. *Mater. Res. Lett.* **7**, 124–130 (2019).
72. Kim, Y., Ballantyne, A. M., Nelson, J. & Bradley, D. D. C. Effects of thickness and thermal annealing of the PEDOT:PSS layer on the performance of polymer solar cells. *Org. Electron.* **10**, 205–209 (2009).
73. Friedel, B. *et al.* Effects of layer thickness and annealing of PEDOT:PSS layers in organic photodetectors. *Macromolecules* **42**, 6741–6747 (2009).
74. Caulfield, D. F. Interactions at the Cellulose-water Interface. *Pap. Sci. Technol. Cut. Edge* 70–88 (1980).
75. Chami Khazraji, A. & Robert, S. Interaction effects between cellulose and water in nanocrystalline and amorphous regions: A novel approach using molecular modeling. *J. Nanomater.* **2013**, (2013).
76. Larsson, O., Said, E., Berggren, M. & Crispin, X. Insulator polarization mechanisms in polyelectrolyte-gated organic field-effect transistors. *Adv. Funct. Mater.* **19**, 3334–3341 (2009).
77. Wang, H., Ail, U., Gabrielsson, R., Berggren, M. & Crispin, X. Ionic Seebeck effect in conducting polymers. *Adv. Energy Mater.* **5**, 1–6 (2015).
78. Ail, U. *et al.* Thermoelectric Properties of Polymeric Mixed Conductors. *Adv. Funct. Mater.* **26**, 6288–6296 (2016).

Acknowledgement

First and foremost, I would really like to thank my God, for providing the opportunity to pursue a master's degree, a decent life, and peace thus far. Furthermore, to my parents, who have always provided moral inspiration and purpose to live life to the fullest. Throughout my studies, I would like to express my gratitude to Prof. Yong Hyun Kim for allowing me to explore and innovate in the organic semiconductor lab, as well as providing me with guidance, support, and inspiration through his advanced and creative thinking.

I'd would like to take this occasion to express my gratitude to all of the professors in the Department of Smart Green Technology Engineering, PKNU for their support and encouragement. For financial support, I am grateful to Pukyong National University and the Brain Korea (BK21) program for awarding me with a scholarship for my studies in Korea.

I'm also grateful to my OSMD lab colleagues including our motherly person Joo Won Han, Jung Ha Kim, Sung Bin Park, Ji Hyun Park, Joo Seung Hyup, Mbak Lia, and Ajenk, who supported me in my research for creating a pleasant and comfortable working atmosphere. In addition, for Indonesian friends Tissa, Rahma, Farris, Sina, Andre, and Mas Jo created an unforgettable experience in Korea.

Lastly, I dedicate all of my achievements to my family and relatives, because their kindness, wisdom, and love have inspired me to achieve every success I've had in my life.

Busan, February 2022

Anky Fitrian Wibowo